International Journal of Engineering Trends and Technology
ISSN: 2231 – 5381 / https://doi.org/10.14445/22315381/IJETT-V70I10P217

Volume 70 Issue 10, 166-187, October 2022

Original Article

An Elite LOA-TFWO Approach for Load-Frequency Control of Islanded Micro-Grids Incorporating Renewable Sources

V. Devaraj[1], M. Kumaresan[2]

[1]*Department of Electrical and Electronics Engineering, Dr. M.G.R Educational and Research Institute, Tamil Nadu, India.*
[2]*Department of Electronics and Communication Engineering, Dr. M.G.R Educational and Research Institute, Tamil Nadu, India*

Corresponding Author : djran14@gmail.com

Received: 21 June 2022 Revised: 22 August 2022 Accepted: 13 October 2022 Published: 20 October 2022

Abstract *- In this paper proposes an intelligent hybrid approach for load-frequency control (LFC) in the islanded micro-grids incorporating various resources like Photovoltaic (PV), Wind Turbine (WT), fuel Cell (FC), Diesel Engine Generator (DEG) and Battery Energy Storage System (BESS). The proposed hybrid approach is the combined implementation of the Lichtenberg Optimization Algorithm (LOA) and Turbulent Flow of Water-based Optimization (TFWO); hence it is named as LOA-TFWO approach. The major objective of the proposed approach is minimizing the change of frequency and maintaining the system's stability. The PID controller is utilized to tune the parameter of the system. With the finite time, the proposed LOA approach generates the data set and the TFWO approach process the outcome of LOA and provides optimal outcome. The proposed approach is executed in the MATLAB/Simulink working platform, and the performances are compared with various existing approaches. Maximum overshoot, steady state error, maximum settling time, integral of frequency error's absolute value in the simulation period, and the objective function is analyzed and compared in the paper. The comparison results reveal that the proposed technique is optimal over the other techniques.*

Keywords *- Load-frequency control, PID controller, Change of frequency, Stability, Lichtenberg optimization algorithm, Turbulent flow of water-based optimization.*

1. Introduction

The conventional power system reliability enhancement, economic improvement and reduction of environmental problems are obtained from introducing microgrid (MG) into the power system [1]. MG is incorporated with a hybrid power generation/energy storage system encompassing various energy resources [2]. Commonly, MGs have used distributed generation units (DGUs) like renewable energy resources (RESs), controllable loads, and storage devices [3]. Distributed generations like wind energy conversion systems, photovoltaic (PV), fuel cells (FCs), diesel engine generators (DEGs), battery energy storage systems (BESSs), and flywheel energy storage systems (FESSs) are commonly utilized in MG studies [4]. The destructive environmental controls and met power consumption spreads are the advantages of distributed generation (DG) [5].

While the connection of multiple energy resources with various energy behaviors causes various issues associated with the control, stability, and performance of MGs [6], the above issues can create a serious problem for the operation of the MG mode [7]. Two modes are present in the MGs operation: islanded mode and grid-connected mode [8]. The grid minimises load disturbances in the grid connection mode instead of islanded mode [9]. As a result, AC-MG must use intelligent and flexible control strategies to achieve strong performance and stability from the linear and unpredictable structure of the RES to the intermittent fluctuations of the RES, the low recession system, the firm references of the DERs and the large load variations [10].

Various reasons must provide system ancillary service provision (SACP) in the island mode as it admits enormous challenges and needs analysis [11]. Within the AC-MG, DERs developing the bulk generation fleet is one of the challenges [12]. This challenge pushes the synchronous generators out of the power system, providing high-frequency deviation [13]. To obtain the appropriate ancillary services providers, such as inertia response and primary frequency response, the technologies based on inverter connection require a proper control approach [14].

MG stability service provision is one of MG's challenges, which can affect the contingency services of MG [15]. If a fault occurs, the change of frequency increases,

which causes the breaking of frequency, oscillating the protection system and the electrical unit's disconnection [16]. Hence, the protection of frequency minimization under low-frequency contingency events must be protected fast [17]. Another challenge is evaluating the impact of energy storage systems, including the DERs [18]. Storage units with non-dispatchable DER units are used to convert them to highly transferable units [19]. Though, the integration of frequency support providers into energy-saving systems is a challenging one. The weak distribution network and this feature increase unbalanced operational levels, thus making the micro-grid control strategy important [20].

This paper proposes an intelligent hybrid approach for load-frequency control (LFC) in the islanded micro-grids incorporating various resources like PV, WT, FC and BESS. The proposed hybrid approach is the combined implementation of the Lichtenberg optimization algorithm (LOA) and Turbulent Flow of water-based optimization (TFWO); hence, it is named as LOA-TFWO approach.

The major objective of the proposed approach is minimizing the change of frequency and maintaining the system's stability. The rest of the paper is organized as follows: Section 2 portrays the recent research work and its background. Section 3 explains the configuration of the microgrid with the proposed hybrid method. The proposed hybrid technique for LFC is explained in 4. Section 5 explains the simulation results and discussion. Section 6 concludes the paper.

2. Recent Research Works: A Brief Review

Multiple research works are available in the literature based on power system load frequency control. K. Lu et al. [21] have suggested that the constrained population is extremely optimised for multi-area interconnected power systems load frequency control. Under the deregulated environment, the Tilted Integral Derivative (TID) controller was utilized to control the area error. Initially, the thermal gas system was considered with two-area and implemented the TID controller.

Various approaches analyzed the introduced TLBO-PS approach. Moreover, the nonlinearity of condition was considered for changing two areas to two areas 6-unit power system. Additionally, the introduced approach performance was increased by connecting Thyristor Controlled Phase Shifter (TCPS) to the tie-line. Moreover, the three-area system utilized Superconducting Magnetic Energy Storage (SMES) devices. H. M. Hasanien and A. El-Fergany [22] have developed the salp swarm algorithm (SSA) for FFC by fine-tuning the gains of proportional-integral-derivative (PID) controllers. The introduced approach was considered the multi-area with the renewable nonlinear power system. By utilizing the TCSC effect, examining the bidirectional power delivery difficulty was the major purpose of the introduced approach. Quasi-oppositional harmony search (QOHS) was also used to minimise the optimization problem. The introduced model considered two thermal units.

A. Fathya and A. M.Kassem [23] have developed the Adaptive Neuro-Fuzzy Inference System (ANFIS) with an antlion optimizer (ALO) for LFC of multi-interconnected system. The Governor unit, turbine with thermal unit, generator and speed regulator unit was present in every area of the power system. The firefly Algorithm (FFA) was utilized to tune the PID controller. The Firefly Algorithm achieved the minimization of settling time and performance improvement.

B. Sonker et al. [24] have suggested the Biogeography Based optimization (BBO) for the LFC problems of multi-area multi-sources power systems. The solar, thermal and wind sources were considered the sources of the two area systems. To obtain the balanced power and regulate the thermal outcome, PI and PID controller was utilized.

The BBO approach tuned the control criteria. Various load perturbation approaches were utilized to determine the system variations. Through the control criteria, the loss of power and the settling time were minimized. P. Sahu et al. [25] have suggested an improved salp swarm optimized type-II fuzzy controller for LFC of multi-area islanded AC microgrid. The FPIDN-FOPIDN controller evaluated the error of the area parameters. The imperialist competitive approach was utilized to achieve less settling time and good performance.

Abazari et al. [26] have suggested the LFC approach for the standalone hybrid microgrid with renewable sources. In isolated micro-gird, the rate of change of frequency (RoCoF) was high. The LFC approach considered various distributed energy resources (DERs) for active power injection. The introduced system was incorporated with a diesel engine generator (DEG), Fuel Cell (FC), Flywheel Energy Storage System (FESS) and Wind Turbine Generator (WTG). Y. Sun et al. [27] have suggested the Robust H∞ and Sliding Mode Control Approach for LFC of multi-area power Systems, including time delay.

The improvement of performance and speed process was achieved by the construction of a sliding surface function. The finite time interval was utilized to guarantee the sliding surface's ability. Linear matrix inequalities were utilized to stabilise the frequency of the multi-area system.

One of the important approaches is Load frequency control to minimize the power-sharing deviation and protect the system from various disturbing factors. Various approaches are introduced for LFC, described in the recent research work. Some of the approaches like Teaching

Learning Based Optimization TLBO, Thyristor Controlled Phase Shifter (TCPS), Superconducting Magnetic Energy Storage (SMES), Thyristor Controlled Series Compensator (TCSC), Quasi Oppositional Harmony Search (QOHS) algorithm, Firefly Algorithm (FFA), Biogeography Based optimization (BBO), State Constrained Distributed Model Predictive Control (SCDMPC), FPIDN-FOPIDN controller etc. are utilized to control the frequency of the load. The main advantage of the TLBO system is that it does not require any algorithm parameters for its operation apart from the population size and iterations at maximum. However, it needs more memory space and time to complete the operation. One of the FACT devices is TCPS which is incorporated with a series and a parallel power transformer. Moreover, TCPS is utilized for optimal power transmission but creates larger amplitude variations and phase errors.

The merits of SMES are high capacity, efficiency, and reliable approach; however, it needs high cost and low power density. TCSC minimises transmission loss through the appropriate series voltage, and the complex constraints-based system faces problems. The firefly Algorithm was an efficient approach and needed less iteration but a high probability of being trapped in local optima. FPIDN-FOPIDN controller reduces the loss of power, but the operation time is high. Therefore, load frequency control using a novel optimization approach is essential for a promising solution to overcome these drawbacks. These disadvantages and issues have motivated me to do this research work.

3. Description of Isolated Microgrid and Preliminaries

The configuration of the isolated microgrid with the proposed approach is shown in Fig 1. The standalone microgrid system is incorporated with a single bus bar, WT unit, PV unit, FC unit, BESS unit and electric loads. The management of the grid is performed by the Distribution Management System (DMS).

Among the DMS [28] and sources, information is transferred in two ways via communication links. The sources of the microgrid are connected via the converters. The circuit breaker is utilized to protect the MG system resources. To protect the system's stability, energy storage systems supply adequate energy for a short time.

The small-signal model of the islanded micro-gird is illustrated in fig 2. The proposed FLC controller is utilized to control the oscillation of frequency. The microgrid frequency oscillation occurs based on the load variation of the microgrid and resources outcome power variation.

Hence, the resources of microgrids are categorized into controllable and uncontrollable sources. WT, PV, and FC are considered uncontrollable sources, and BEES with distributed energy generation are controllable resources. Here, the predictable disturbances are the disturbances occurring based on the variation of uncontrollable resources. Unpredictable disturbances are considered variations of load.

3.1. PV Unit Modeling

PV unit is modeled based on the arrangement of a combination of parallel and series-coupled PV cells. The output energy is obtained based on the series and parallel arrangement of the PV cell. The PV cell's input is solar radiation, which produces the output energy. The PV cell output is described as,

$$P_{PV}^{*} = \eta A_P \wp (1 - 0.005(t_e + 25) \quad (1)$$

Here, irradiation of the solar is denoted as$\wp$, the efficiency of panels energy conversion is denoted asη , area of panels is denoted asA_P, and temperature in Celsius is denoted ast_e. The PV outcome varies because the efficiency and area are constant and based on the temperature and irradiation. The PV unit simplified transfer function is described as,

$$G_{PV}^{*} = \frac{K_{PV}}{1+st_{PV}} \quad (2)$$

Here, PV panel gain and time constant are denoted asK_{PV},t_{PV}.

3.2. WT Unit Modelling

Based on the speed of the wind, the output power of WT is present. The speed characteristics of wind are modeled based on Weibull PDF. The speed of wind is described as

$$F_W(h) = \left(\frac{2h}{(h_i)^2}\right) exp^{\left(-\left(\frac{h}{h_i}\right)^2\right)} \quad (3)$$

Here, wind speed is expressed as$h$; the scale index is indicated ash_i. The average speed of wind is expressed as,

$$h_{Avg} = \int_0^{\infty} hF_W(h)dh = \left(\frac{\sqrt{\pi}}{2}\right) h_{iI} \quad (4)$$

The output power of wind turbine is described as,

$$P_{WT}^{*}(h) = \begin{cases} 0, \rightleftarrows h \le h_{CutI} \rightleftarrows or h \ge h_{CutO} \\ P^{Rate}\left(\frac{h-h_{CI}}{h_R-h_{CI}}\right), h_{CutI} \le h \le h_{Ra} \\ p^{Rate}, h_{Ra} \le h \le h_{CutO} \end{cases} \quad (5)$$

Here, the cut-in speed, cut-off speed and rated speed of the wind turbine are expressed as$h_{CutI} \rightleftarrows$,$h_{CutO}$,$h_{Ra}$ respectively.

The WT unit simplified transfer function is described as,

$$G_{WT}^{*} = \frac{K_{WT}}{1+st_{WT}} \quad (6)$$

Here, WT panel gain and time constant are denoted asK_{WT},t_{WT}.

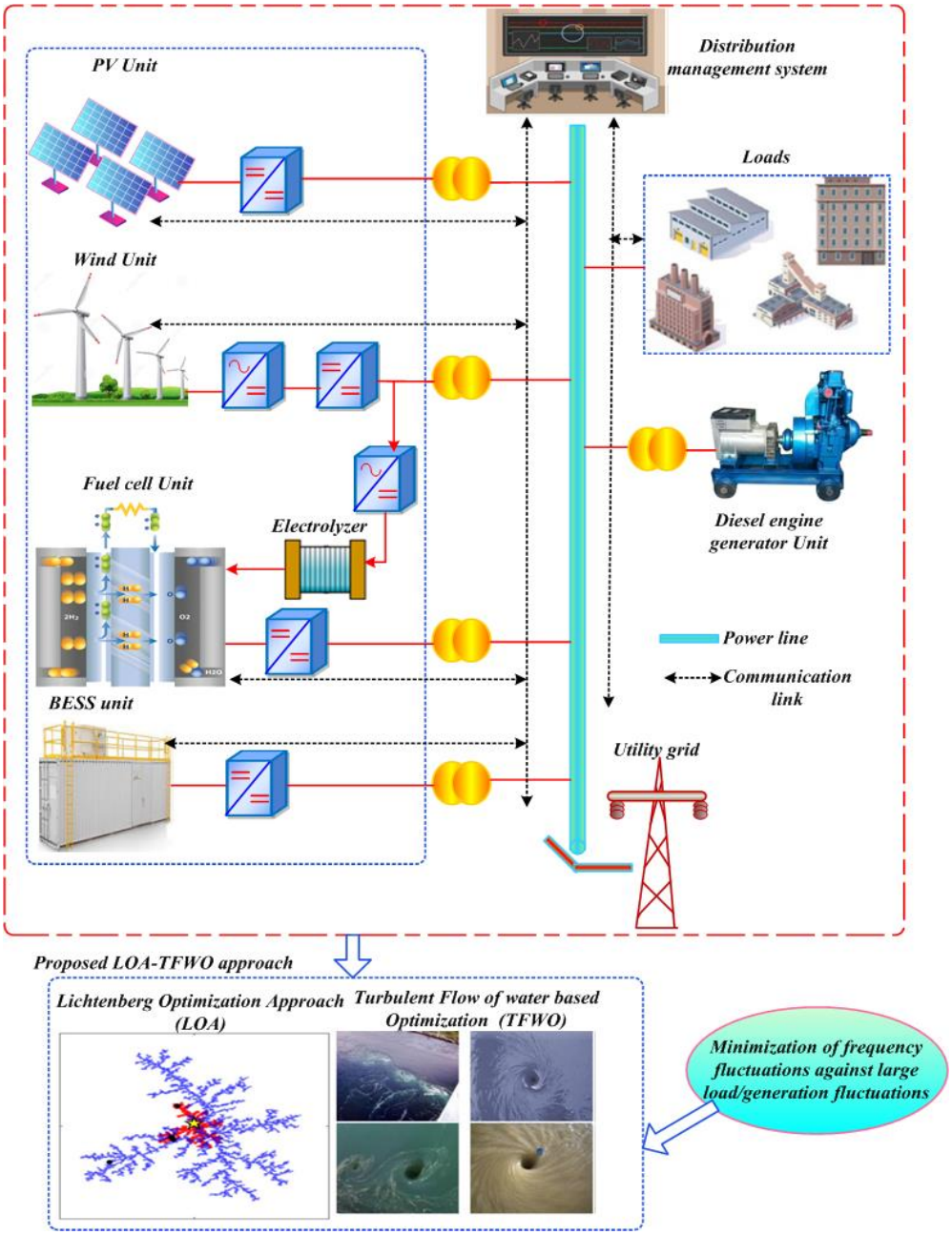

Fig 1. Configuration of the isolated microgrid with the proposed approach

3.3. FC Unit Modelling

The fuel cell generates energy based on the conversion of chemical energy into electrical energy. Like the battery process, FC is operating. Nevertheless, FC continuously produces the dc power until the hydrogen and oxygen supply. FC is utilised in the distributed generation system because of its effectiveness, flexibility and simple operation. The voltage of the fuel cell is described as,

$$V_{FC}^{*} = N_{FC}\left[v_0 + \frac{\tau_g T}{2F}\left(ln\left(\frac{P_{H_2}P_{O_2}^{1/2}}{P_{H_2O}}\right)\right) - r_i I_{FC}\right] \qquad (7)$$

Here, the number of fuel cells connected in series is indicated as N_{FC}, the universal gas constant is expressed as τ_g, free energy voltage is expressed asv_0 , the temperature is expressed as T, the current through the fuel cell stack is expressed as I_{FC} , Faraday constant is expressed as F , partial pressures of hydrogen, water and oxygen are expressed as P_{H_2}, P_{O_2}, P_{H_2O} respectively.

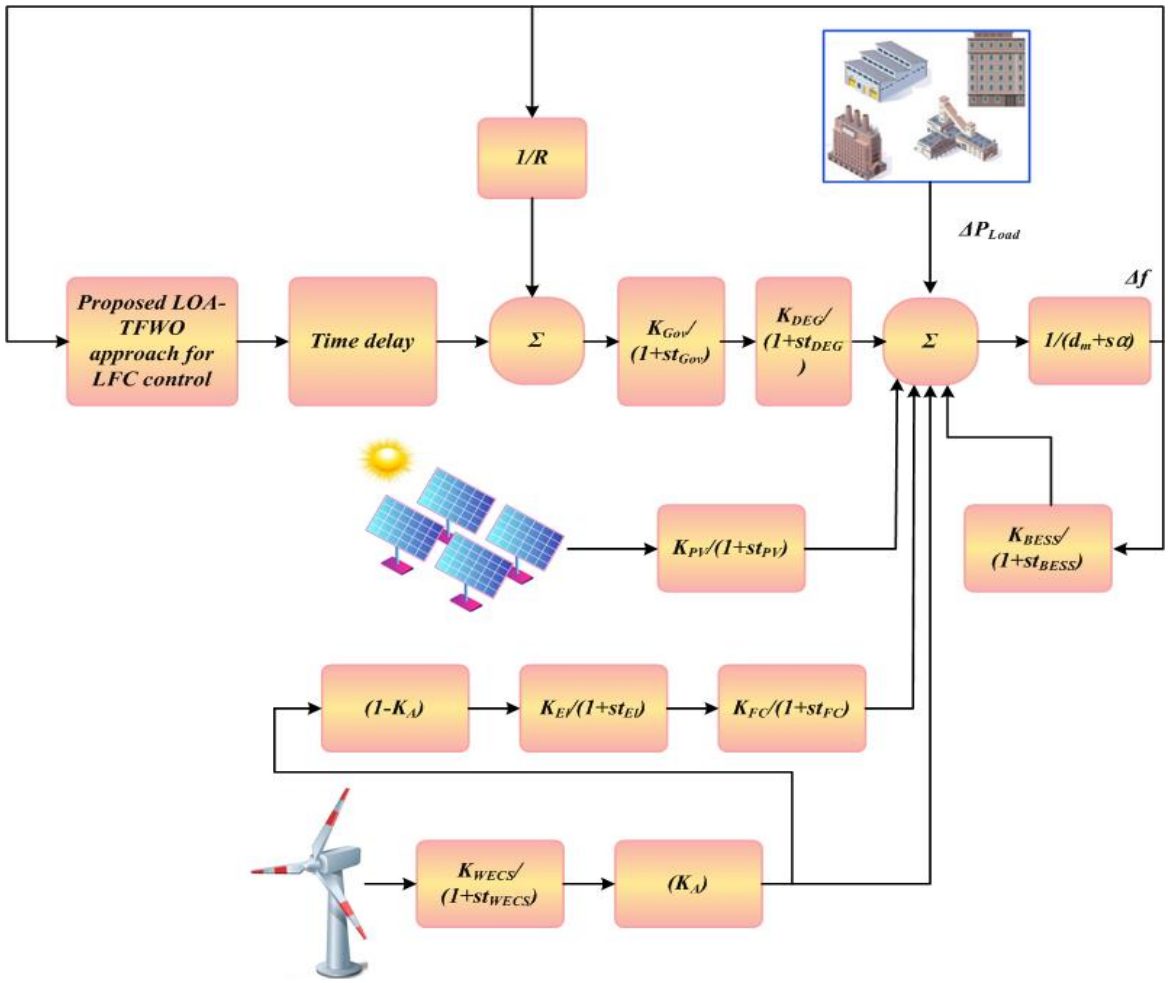

Fig. 2 The small-signal model of the islanded micro-gird

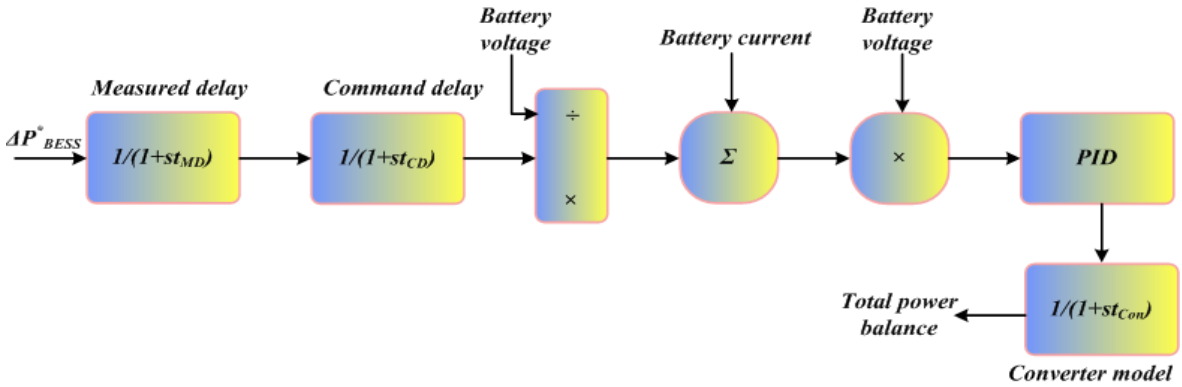

Fig. 3 BESS in FLC

The first-order transfer function of the fuel cell is described as,

$$G_{FC}^{*} = \frac{K_{FC}}{1+st_{FC}} \quad (8)$$

Here, t_{FC} and K_{FC} represented as the fuel cell time constant and gain, respectively.

3.4. BESS Unit Modelling

Energy storage technologies are evaluated by various approaches [29]. For example, consider the energy storage system, like a simple black box and steady-state magnitudes obtained by some mathematics equation using inputs. When the load is varying, then the BESS provides constant output voltage.

Therefore some delay is occurring. There are three types of delay: measurement delay, command delay, and converter delay. The active power imbalance is minimized by the PID controller based on BESS. Fig 3 displays the BESS in FLC.

3.5. Converter Modelling

The converters are utilized to control the flow of current in a bi-direction when the extra power is charged to the battery [30]. Moreover, it provides the necessary power from the DC source to the load. The required number of converters is described as,

$$N_{Con} = \frac{P_G^{Max}}{P_{Con}^{Max}} \tag{9}$$

Here, the maximum power generated by the energy sources is expressed asP_G^{Max} , and the maximum power of the converter is expressed asP_{Con}^{Max}.

3.6. PID Controller Modelling

Proportional-integral-derivative (PID) controller [31-33]is widely utilized in the industries. It is utilized to compute the parameter's tuning and minimise the system's error. The error is calculated from the reference and actual value of the system. The PID controller transfer function is described as,

$$U(t) = K_p E(T) + K_i \int_0^t E(\varsigma)\, d\varsigma + K_d \frac{dE}{dt} \tag{10}$$

$$E = R - y \tag{11}$$

Here, control error is denoted as$E$. The parameterized controller is described as,

$$U(t) = K_p \left[E(T) + \frac{1}{t_i}\int_0^t E(\varsigma)\, d\varsigma + t_d \frac{dE(T)}{dT}\right] \tag{12}$$

Here, integral time is denoted ast_i, derivative time denoted ast_d.

3.7. Dynamic MG Modeling

The dynamic equation of MG [34] is described as,

$$\overset{*}{X} = aX + bU + cE_D \tag{13}$$

Here, the state of the system is considered as$X(T) = [X_1^T \quad X_{21}^T]^T, X_1 = \Delta f \in Z\, X_2 = [\Delta p_{DEG} \quad \Delta P_{BESS}]^T \in Z^3$. The control input of the system is described as

$$U(T) = [\Delta U_{DEG} \quad \Delta U_{BESS}]^T \in Z^3 \tag{14}$$

The external disturbance is described as,

$$E_D = \Delta p_{FC} + \Delta p_{WT} + \Delta p_{PV} - \Delta p_{Load} \in Z^3 \tag{15}$$

The matrix at appropriate dimensions is described as,

$$c = \begin{bmatrix}\frac{1}{H} & 0 & 0 & 0\end{bmatrix}^T, a = \begin{bmatrix}a_{11} & a_{12}\\ a_{13} & a_{14}\end{bmatrix}, b = \begin{bmatrix}0\\ b_2\end{bmatrix} \tag{16}$$

Here, $a_{11} = -\frac{c}{H}, a_{12} = -\frac{1}{H}[1 \quad 1 \quad 1]$,

$$a_{21} = \begin{bmatrix}-\frac{K_{DEG}}{Zt_{DEG}} & 0 & 0\end{bmatrix} a_{22} = Diag\left[-\frac{1}{t_{DEG}} \quad -\frac{1}{t_{BESS}} \quad -1\right],$$

Here, Has inertia constant, the non-singular matrix is described as,

$$b_2 = Diag\left[\frac{K_{DEG}}{t_{DEG}} \quad \frac{K_{BESS}}{t_{BESS}} \quad \frac{1}{t_{BESS}}\right] \in Z^{3\times 3} \tag{17}$$

The system is described below equation,

$$X_1 = a_{11}X_1 + a_{12}X_2 + \frac{1}{H}E_D \tag{18}$$

$$X_2 = a_{21}X_1 + a_{22}X_2 + b_2U \tag{19}$$

If the upper bound of $E_D$is u_1, then it described as $|E_D| \le u_1$

3.8. Network and Load State-Space Model

The network and load, small-signal state-space model [35,36] is described here. There are various numbers of loads $L$and network node N, and the number of lines is denoted as LN; the state-space equation of the load is described as,

$$\Delta i_{Load}^{dq} = A_{Load}\left[\Delta i_{Load}^{dq}\right] + B_{Load}\left[\Delta v_B^{dq}\right] \tag{20}$$

For the load is connected from one node to another, then,

$$\Delta i_{Load}^{dq} = \left[\Delta i_{Load}^{dq1}\Delta i_{Load}^{dq2}\ldots\Delta i_{Load}^{dqL}\right]^T \tag{21}$$

Here, $A_{Load} = \begin{bmatrix}-\frac{R_{load\rightarrow i}}{L_{Load\rightarrow i}} & f\\ f & -\frac{R_{Load\rightarrow i}}{L_{Load\rightarrow i}}\end{bmatrix}, B_{Load} = \begin{bmatrix}\frac{1}{L_{Load\rightarrow i}} & 0\\ 0 & \frac{1}{L_{Load\rightarrow i}}\end{bmatrix}$

The state space equation of the network is described as,

$$\Delta i_{Line}^{dq} = A_{Tot}\left[\Delta i_{Load}^{dq}\right] + B_{Tot}\left[\Delta v_B^{dq}\right] \tag{22}$$

At the ith line, the network is described as,

$$\Delta i_{Load}^{dq} = \left[\Delta i_{Tot}^{dq1}\Delta i_{Tot}^{dq2}\ldots\Delta i_{Tot}^{dqL}\right]^T \tag{23}$$

Here, $A_{Tot,i} = \begin{bmatrix}-\frac{R_{Line\rightarrow i}}{L_{Line\rightarrow i}} & f\\ f & -\frac{R_{Line\rightarrow i}}{L_{Line\rightarrow i}}\end{bmatrix}$,

$$B_{Tot,i} = \begin{bmatrix} \cdots & \frac{1}{L_{linei}} & 0 & \cdots & -\frac{1}{L_{linei}} & 0 & \cdots \\ \cdots & 0 & \frac{1}{L_{linei}} & \cdots & 0 & -\frac{1}{L_{linei}} & \cdots \end{bmatrix}$$

(31)

Here, lower and upper limits of power generation are denoted as$P_{Min}^{DER_i}$,$P_{Max}^{DER_i}$. The BESS stored energy is restricted by the maximum and minimum capacity of storage, which is described as,

$$E_{Min}^{BESS} \leq E_T^{BESS} \leq E_{Max}^{BESS} \tag{32}$$

3.9. Microgrid Overall Modeling

The whole model of the inverter, network, and load joined to form the overall microgrid, which model is described in this section [37,38]. For each model, the input is voltage. The node voltage is described as,

$$\Delta v_B^{dqi} = R_N\left[\Delta i_o^{dqi} - \Delta i_{Load}^{dqi} \ldots \Delta i_{Tot}^{dqi}\right] \tag{24}$$

The node voltage is described as,

$$\Delta v_B^{dqi} = R_N\left[M_{INV}[\Delta i_o^{dqi}] + M_{Load}[\Delta i_{Load}^{dqi}] + M_{Tot}[\Delta i_{Tot}^{dqi}]\right] \tag{25}$$

Here, the diagonal matrix asR_N, the direction of the node current asM_{Tot}. The overall small-signal state-space model of the microgrid is described as

$$\begin{bmatrix} \Delta \overset{*}{x}_{INV} \\ \Delta i_{Line}^{dq} \\ \Delta i_{Load}^{dq} \end{bmatrix} = A_{MG} \begin{bmatrix} \Delta x_{INV} \\ \Delta i_{Line}^{dq} \\ \Delta i_{Load}^{dq} \end{bmatrix} \tag{26}$$

3.10. Objective Formulation

The major objective of the proposed approach is minimizing the frequency oscillation under large load and generation fluctuation, which means reducing exact variations of state and control vectors with specific periods. The objective function is described as,

$$Obj = Min\{K_1 \times F_1 + K_2 \times F_2\} \tag{27}$$

$$F_1 = \int_0^T (|X_1| + |X_2| + |X_3| + |X_4|)\, dT \tag{28}$$

$$F_2 = \int_0^T (|U_1| + |U_2| + |U_3|)\, dT \tag{29}$$

3.11. Operating Constraints of the System

This paper considers the constraints like output power of DERs like PV, WT, FC, stored energy in BESS and MG power balance [39,40]. The total power produced by DERs, energy stored in BESS, meets the total MG necessity, which is satisfied at each time interval. The power balance constraints are expressed as,

$$L(t) = \sum_T P_{PV}^* + P_{WT}^* + P_{FC}^* + P_{BESS}^* \tag{30}$$

$$P_{Min}^{DER_i} \leq P_T^{DER_i} \leq P_{Max}^{DER_i}$$

4. Proposed LOA-TFWO Approach-Based Load Frequency Control

This paper proposed a hybrid LOA-TFWO approach for LFC of a standalone hybrid microgrid with RESs. Due to the unpredictable structure and the intermittent fluctuations of the RES, the operation of the isolated microgrid have some problems. In the isolated microgrid, frequency oscillation is high [41]. So to reduce the problem, here is the proposed LOA-TFWO approach. The small signal dynamic model is utilized in the isolated microgrid. Here consider the resources like PV, WT, FC, and BESS.

The proposed hybrid approach is the combined implementation of the Lichtenberg Optimization Algorithm (LOA) and Turbulent Flow of Water-based Optimization (TFWO); hence it is named as LOA-TFWO approach. PID controllers have utilized the tune of the parameter of the system. The LOA approach is utilized to generate the dataset of the system, and the TFWO approach processes parameters.

4.1. Lichtenberg Optimization Algorithm (LOA) Based Gain Parameter Optimization

One of the metaheuristic optimization approaches is the Lichtenberg Optimization approach which is inspired by the physical event of radial propagation of intra-cloud lightning. The Lichtenberg Figures (LF) [42] are the sky's images because of the lightning. LF offers significant properties due to the superior structure shapes. Hence, through the utilization of these figures, the population of LOA is scattered to the small branches. Therefore, this algorithm is developed that distributes its number by the main number and its branches.

In this paper, the gain parameters are optimized by the LOA approach. The step-by-step process of LOA is described as follows,

4.1.1. Step 1: Initialization

Initialize the gain parameters like $k_P, k_i, k_d$of the PID and the limits, microgrid structural data, parameters of LOA, and iteration of the system.

4.1.2. Step 2: Random Generation

Generate the LF using the routine parameter m, then the population of PID is randomly generated by,

$$Ra = \begin{bmatrix} (pid)_{11} & (pid)_{12} & \cdots & (pid)_{1n} \\ (pid)_{21} & (pid)_{22} & \cdots & (pid)_{2n} \\ \vdots & \vdots & \vdots & \vdots \\ (pid)_{m1} & (pid)_{m2} & \cdots & (pid)_{mn} \end{bmatrix} \quad (33)$$

4.1.3. Step 3: Apply rotation in LF

When the reference speed is not equal to zero, then the next LF is created based on the rotation.

4.1.4. Step 4: LF Triggering

In this step, the LF is triggered first and obtains the optimum point of the previous one. It continues to obtain the best fitness

4.1.5. Step 5: Evaluates the Fitness

The fitness is evaluated at some point in the Lichtenberg figures. Determine the best optimal value. The fitness functions are evaluated based on the objective function

$$F = Min[E_S(t)] \quad (34)$$

Here, the error function is described as $E_S(t)$

4.1.6. Step 6: Determine the lowest point

Determine the best value in the search space.

4.1.7. Step 7: Stopping Criteria

The optimal outcome is obtained, then stops the process; otherwise, go to step 3. The best parameter is found by,

$$\begin{bmatrix} F_{11} & F_{12} & \cdots & F_{1n} \\ F_{21} & F_{22} & \cdots & F_{2n} \\ \vdots & \vdots & \vdots & \vdots \\ F_{m1} & F_{m2} & \cdots & F_{mn} \end{bmatrix} = \begin{bmatrix} (pid)_{11} & (pid)_{12} & \cdots & (pid)_{1n} \\ (pid)_{21} & (pid)_{22} & \cdots & (pid)_{2n} \\ \vdots & \vdots & \vdots & \vdots \\ (pid)_{m1} & (pid)_{m2} & \cdots & (pid)_{mn} \end{bmatrix} \quad (35)$$

The optimal parameter is used to process the TFWO approach.

4.2. Turbulent Flow of Water-Based Optimization (TFWO) Based Load Frequency Control

The TFWO is an effective collection-to-optimization mechanism that is used to include the whirlpools that are formed in the turbulent water flow. Suppose the TFWO has a permanent structure that removes the issues for selecting the control parameters. It is used to increase the convergence speed [43-47]. The random characteristic of nature is another wise called the whirlpool, which happens in seas, rivers and oceans. The whirlpool centre acts like a sucking hole as well as particles and pulling objects, and it is around towards its centre and the interior, and it is means by applying centrifugal force on them. The whirlpool forms the small ridges on the surface of the streamlet apart from each other.

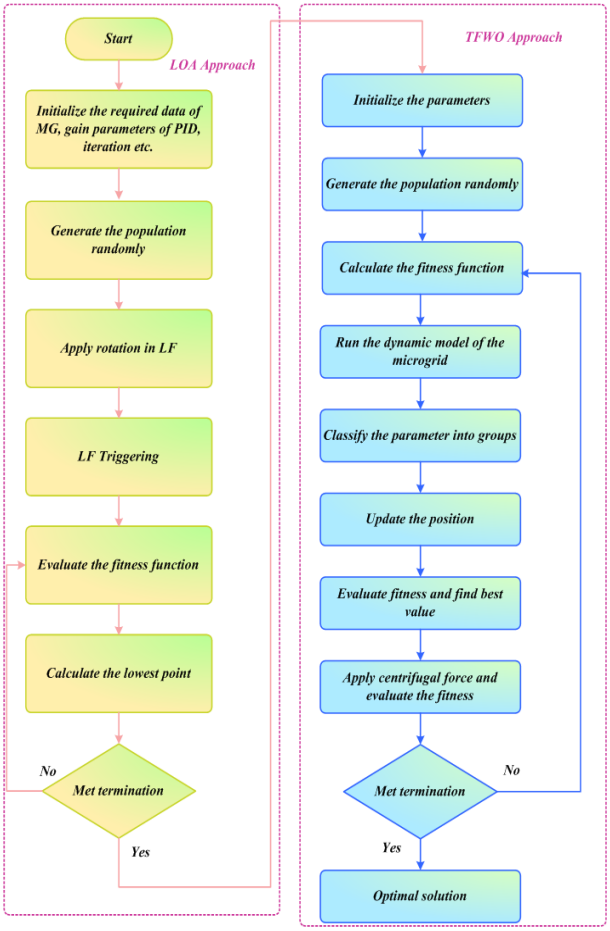

Fig 4. Flow chart of proposed LOA-TFWO approach

The flowing of water collides with the ridges and moves around itself, as the water moves around itself on the ridges in a narrow path, and it slowly merges around from the circle to shape a funnel. Control of the frequency and increase the system stability is obtained by the TFWO approach. The step-by-step process is given below,

4.2.1. Step 1: Initialization

The data set of the LOA outcome is given to the input of TFWO

4.2.2. Step 2: Random Generation

Create the matrix of data set randomly based on load demand. The random solution is described as,

$$K_i = \begin{bmatrix} k_{11} & k_{12} & \ldots & k_{1n} \\ k_{21} & k_{22} & \ldots & k_{2n} \\ \vdots & \vdots & \vdots & \vdots \\ k_{m1} & k_{m2} & \ldots & k_{mn} \end{bmatrix} \quad (36)$$

4.2.3. Step 3: Fitness Function

Determine the fitness function based on the objective

$$F_i = Obj(Min\{K_1 \times F_1 + K_2 \times F_2\}) \quad (37)$$

4.2.4. Step 4: Classification

Classify the population of MG into a number of groups, and the best fitness function is called whirlpool, which pulls the objects. The object consists of the number of population and number of whirlpools (Wh_j).

4.2.5. Step 5: Update the Position

The new position of the objective is described as,

$$K_i^{new} = Wh_j - \Delta K_i \quad (38)$$

$$\Delta K_i = \left(cos(\delta_i^{new}) * R(1,d) * \left(Wh_f - K_i\right)\right) \quad (39)$$

4.2.6. Step 6: Evaluate the Fitness

The following equation evaluates the updated functions,

$$K_i^{new} = min(\, max(\, K_i^{new}, K^{min^{max}} \quad (40)$$

4.2.7. Step 7: Centrifugal Force

Apply the centrifugal force, which moves the parameters towards the objective function, which is described as

$$K_i^{new} = ((cos(\delta_i^{new}))^2 * (sin(\delta_i^{new}))^2)^2 \quad (41)$$

4.2.8. Step 8: Evaluate the Fitness of Whirlpool

Evaluate the whirlpool fitness

$$Wh_j^{new} = min\left(max\left(Wh_j^{new}, K^{min}()^{max}\right)\right) \quad (42)$$

4.2.9. Step 9: Check the Best Value

Check any new object in a whirlpool or group which has a better fitness than that of the whirlpool, then replace the whirlpool with the best one in the following way,

$$f(Wh_j) \leftrightarrow f(K_{best}) \quad (43)$$

Using this way best value is achieved.

4.2.10. Step 10: Termination Criteria

If met the termination criteria, then achieve the best value; otherwise, go to step 5. Fig 4 shows the flowchart of the proposed LOA-TFWO approach.

5. Results and Discussion

This section describes the performance of the proposed system. The proposed hybrid LOA-TFWO is utilized to control the frequency variation of load. The proposed approach is simulated in the MATLAB Simulink platform.

The microgrid is incorporated with various sources. The system's performance is analyzed based on the load changes and power variation of PV and wind units. There has a large disturbance that occurs due to the load and RES. The proposed approach is also analyzed based on the state variables and the control inputs. The proposed approach is utilized three PID controllers.

5.1. Case 1: Performance Analysis of Proposed Approach Based On the State and Control Variables

Analysis of variations of the micro-grid's load is shown in fig 5. The load power starts at 1 W at 0 to 50 sec, then decreases to 0.6 W at 50 to 100 sec. After that, it decreased to 0.5 W at 100 to 175 sec, after it increased to 0.7 W at 175 to 225 sec. Again it increased to 0.9 W at 225 to 300 sec. Analysis of power variations of the WT is displayed in fig 6. The WT power is constant at 0.4 W at 0 to 195 sec, then decreases to 0.2 W at 195 to 240 sec. After that, it increased to reach 0.69 W at 240 to 300 sec. Analysis of power variations of the PV is displayed in fig 7.

The PV power starts at 0.475 W at 0 to 25 sec and then decreases to 0.2 W at 25 to 75 sec. After that, it increased to reach 0.475 W at75 to 150 sec. Again it decreased to 0.2 W at 150 to 300 sec. Analysis of state variables in the LFC of PID1, PID 2, and PID 3 is displayed in fig 8. Subplot 8 (a) shows the state variables in the LFC of PID1.

Initially, it oscillates from 0 to 290 at0 to 10 sec. After that, it increased to 90 at 50 sec. Then it decreased to -125 at 100 to 150 sec. After that, it increased to 90 at 240 sec. Then it decreased to 0 at 250 to 300 sec. Subplot 8 (b) shows the state variables in the LFC of PID2. Initially, the state variable of PID 2 oscillated from -5 to 7 at 0 to 5 sec, then decreased to 0. Then the oscillation occurs at 50, 100, 175, and 225. This oscillation occurs below the -2 to 2 state variable. Subplot 8 (c) shows the state variables in the LFC of PID3. Initially, the state variable of PID 3 oscillated from -5 to 7 at 0 to 5 sec, then decreased to 0. Then the oscillation occurs at 50, 100, 175, and 225. This oscillation occurs below the -2 to 2 state variable.

Analysis of control input in LFC of PID1, PID 2, and PID 3 is displayed in fig 9. Subplot 8 (a) shows the control input in the LFC of PID1. Initially, it oscillates from -0.7 to 0.5 at 0 to 10 sec. After that, it decreased to 0. Then the oscillation occurs at 50, 100, 175, and 225. At the time of 50, the input oscillates from -0.2 to 0.3, and at the time period of 100, the input oscillates from -0.02 to 0.03. At 175 and 225 sec, the oscillation occurs around -0.1 to 0.1. Subplot 8 (b) shows the control input in the LFC of PID2. Initially, the control input of PID 2 oscillated from -0.5 to 0.6 at 0 to 10 sec, then decreased to 0. Then the oscillation occurs at 50, 100, 175, and 225. This oscillation occurs below the -0.2 to 0.2 control input. Subplot 8 (c) shows the control input in the LFC of PID3. Initially, the control input of PID 3 oscillated from -0.7 to 0.5 at 0 to 5 sec, then decreased to 0. Then the oscillation occurs at 50, 100, 175, and 225. This oscillation occurs below the -2 to 2 state variable.

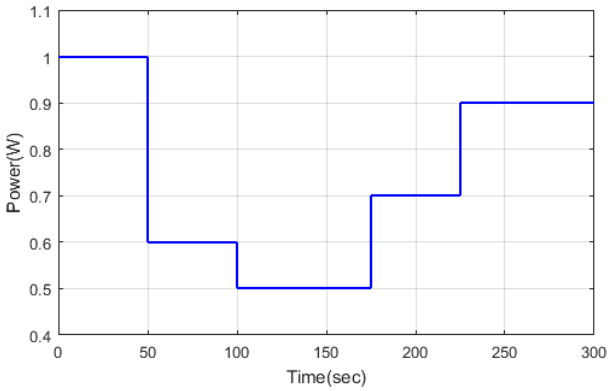

Fig. 5 Variations of micro-grid's load

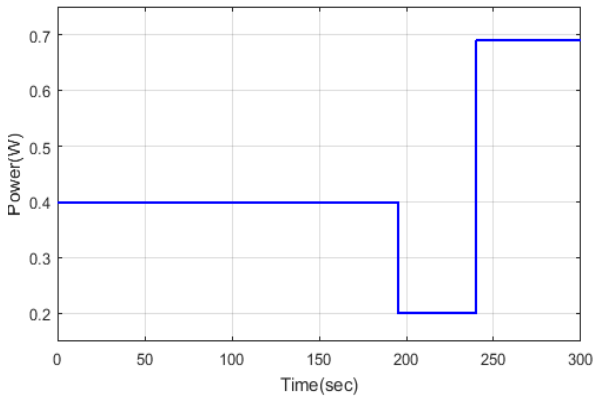

Fig. 6 Power variations

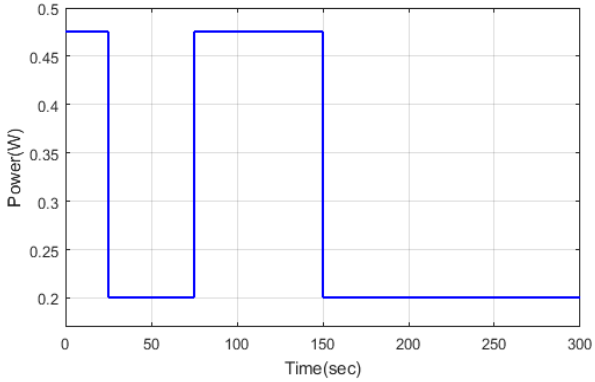

Fig. 7 Variations of the PV

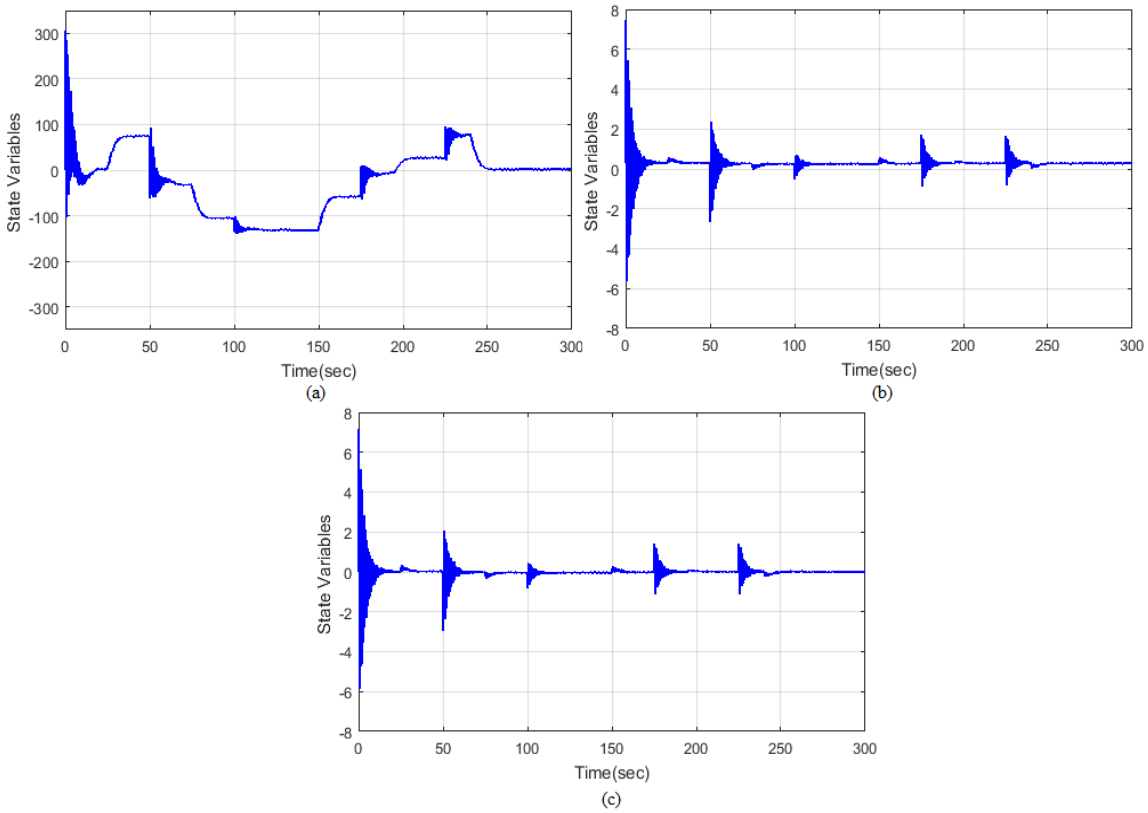

Fig. 8 Analysis of state variables in LFC of (a) PID1, (b) PID 2, (c) PID 3

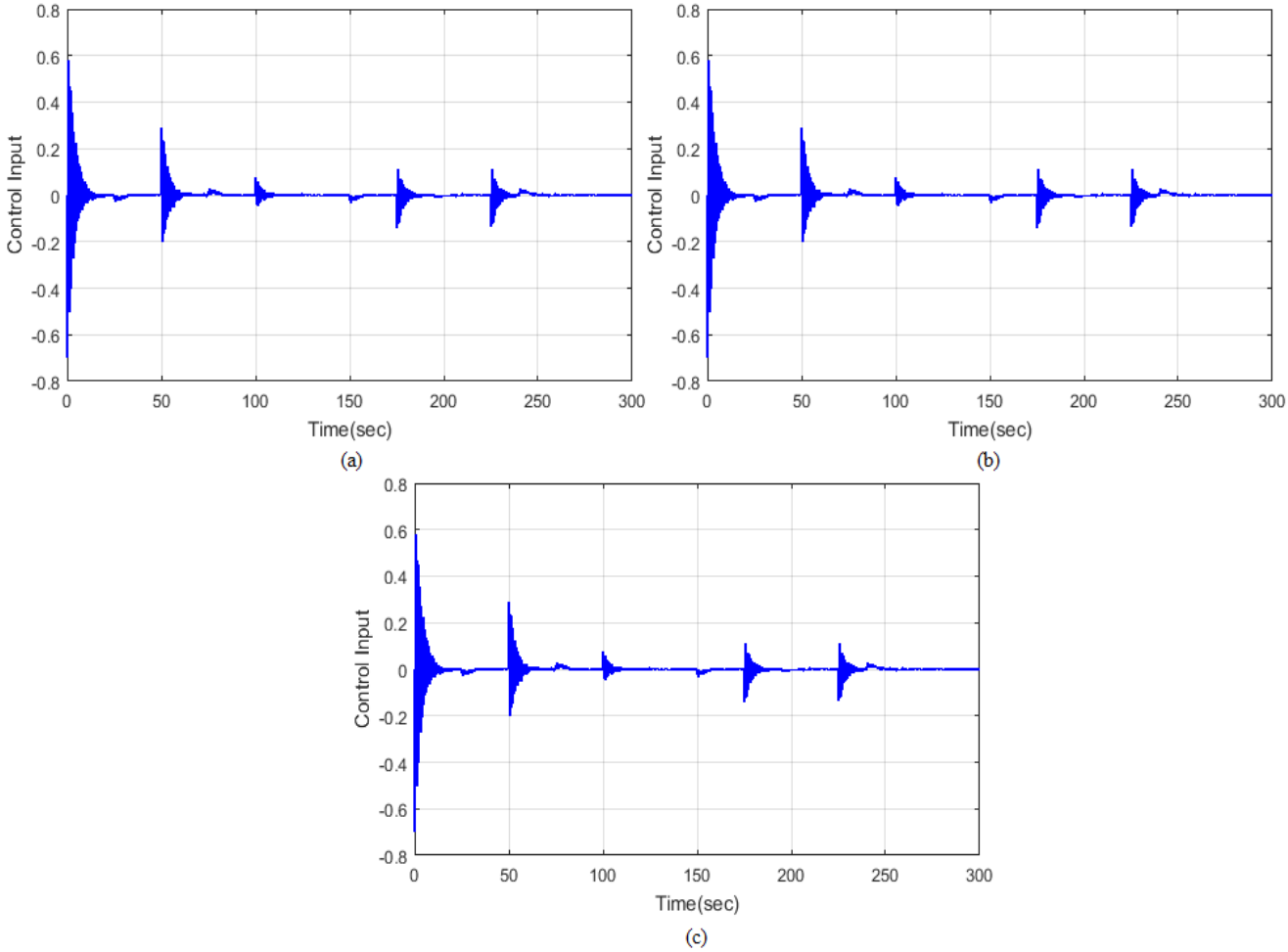

Fig. 9 Analysis of control input in LFC of (a) PID1, (b) PID 2, (c) PID 3

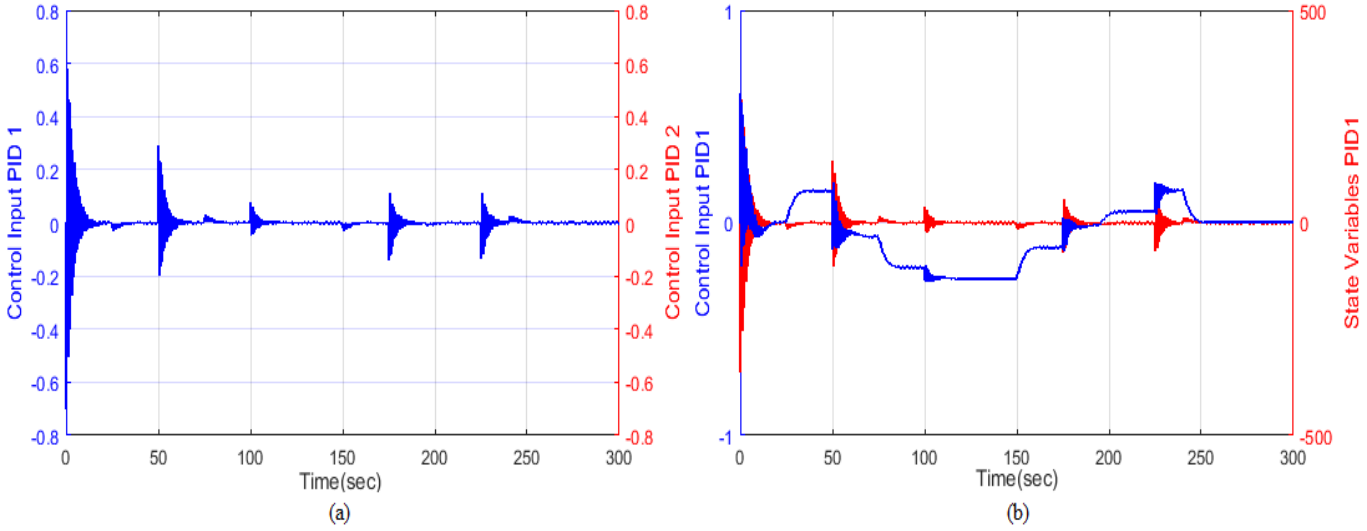

Fig. 10 Analysis of LFC at (a) control input of PID 1 and control input of PID 2 doubly, (b) Control Input PID 1 and state variable 1-doubley

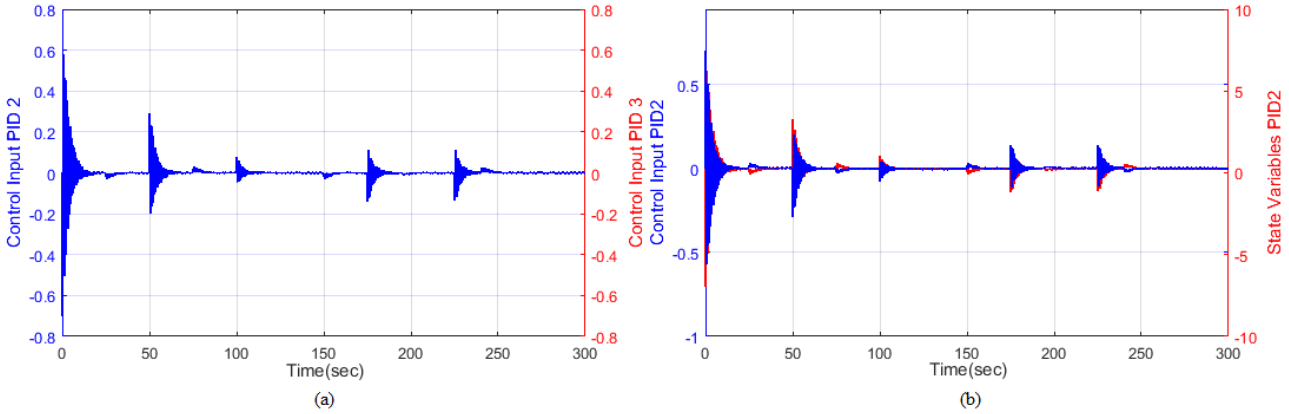

Fig. 11 Analysis of LFC at (a) control input of PID 2 and control input of PID 3 doubly, (b) Control Input PID 2 and state variable 2-doubley

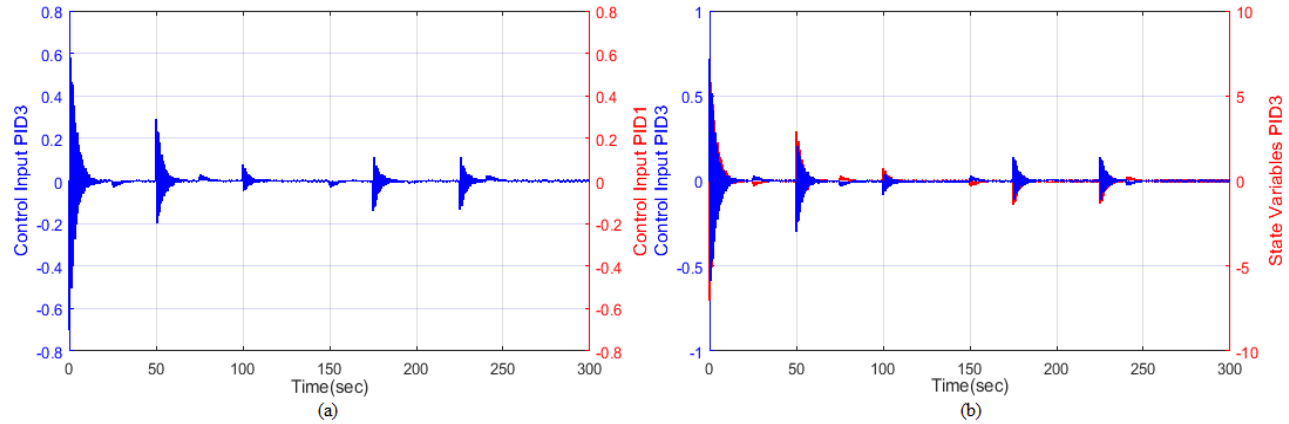

Fig. 12 Analysis of LFC at (a) control input of PID 3 and control input of PID 1 doubly, (b) Control Input PID 3 and state variable 3-doubley

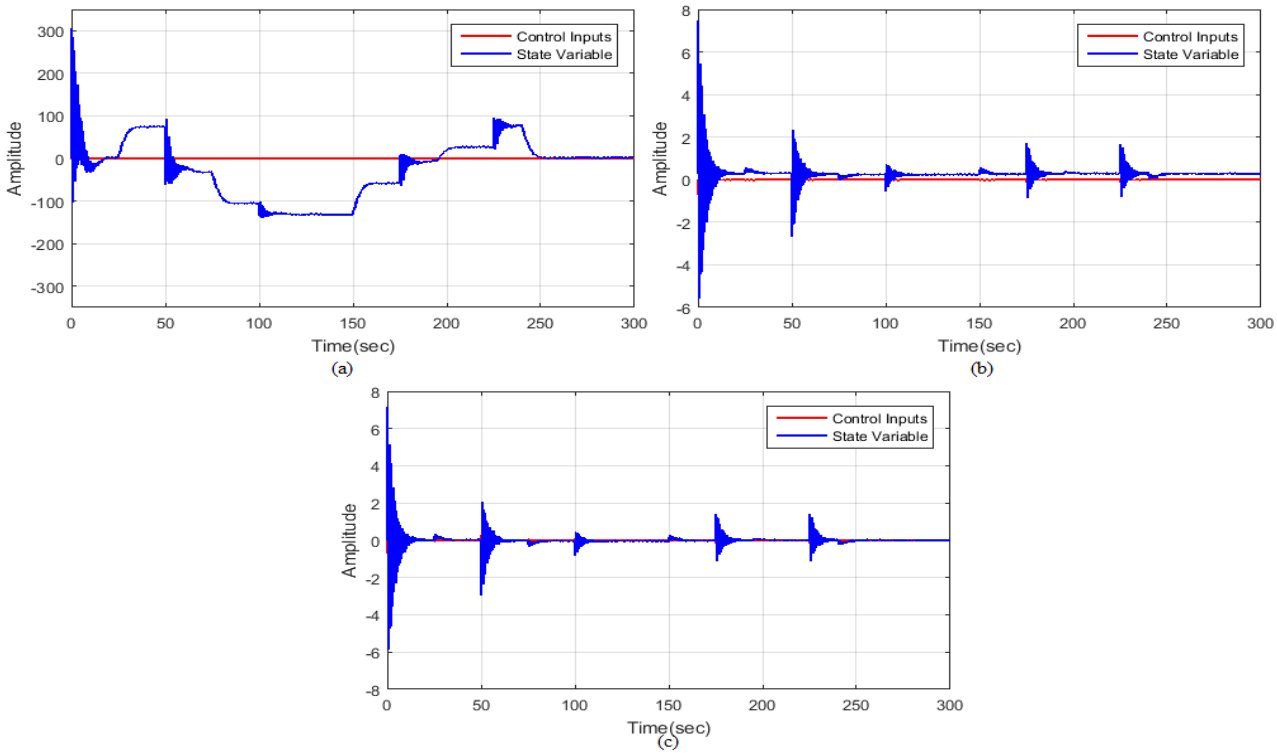

Fig. 13 Analysis of LFC at (a) Analysis of LFC at control input1 and state variable 1, (b) Control input 2 and state variable 2, (c) Control input3 and state variable 3

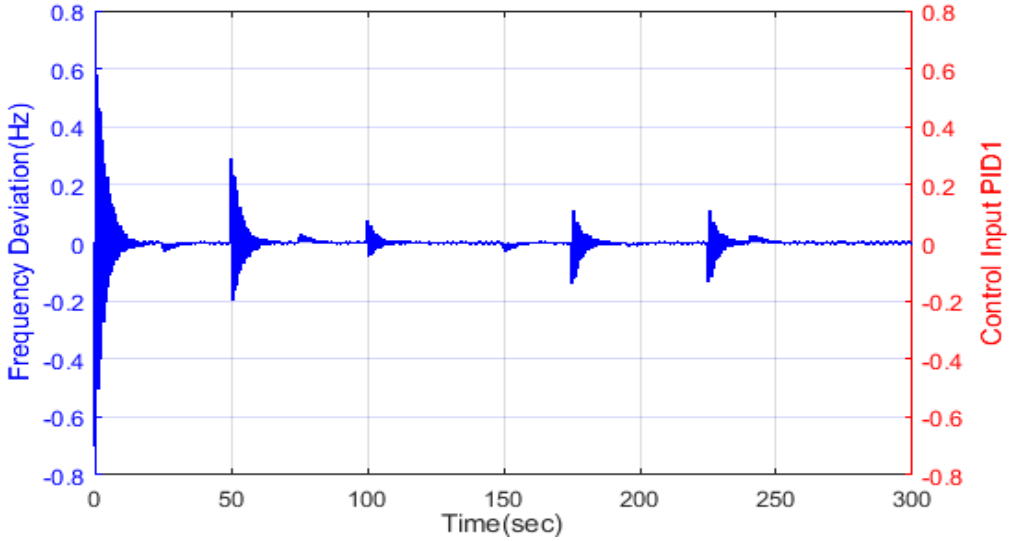

Fig. 14 Analysis of LFC using proposed LOA-TFWO Frequency and control input PID 1-doubley

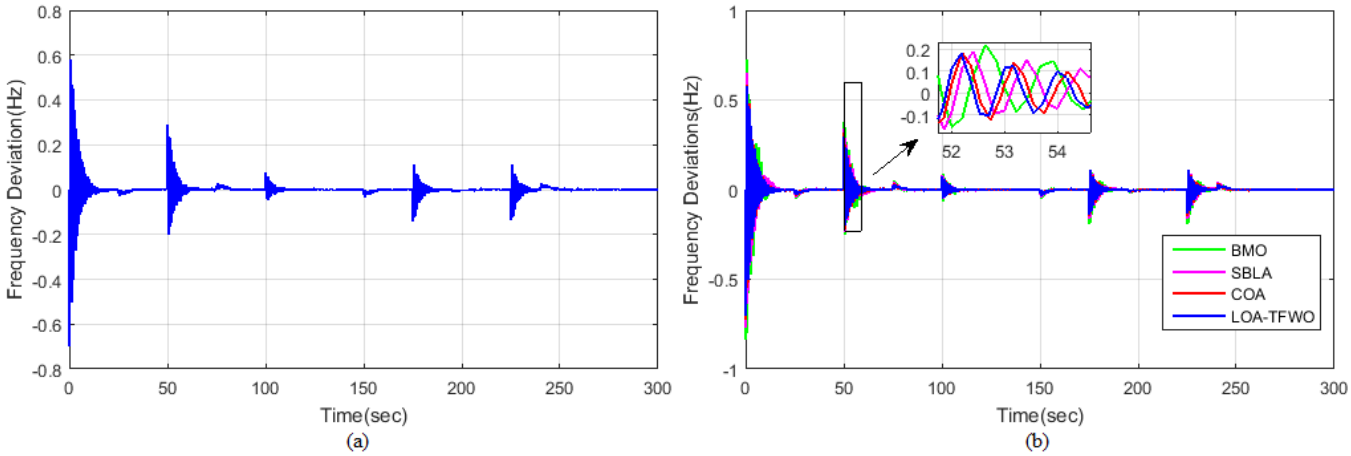

Fig. 15 Analysis of (a) Frequency deviation (b) Comparison of frequency deviation with various approaches

Fig 10 analysis the control input of PID 1 and control input of PID 2 doubly and control Input PID 1 and state variable 1-doubley. Subplot 10 (a) shows the control input in LFC of PID1 and PID 2 doubly. The control input PID 1 oscillates -0.7 to 0.5 at 0 to 10 sec. After that, it decreased to 0. Then the oscillation occurs at 50, 100, 175, and 225. At the time of 50, the input oscillates from -0.2 to 0.3, and at the time period of 100, the input oscillates from -0.02 to 0.03. At 175 and 225 sec, the oscillation occurs around -0.1 to 0.1.

Subplot 10 (b) shows the control input in LFC of PID1 and state variable 1-doubley. Initially, the control input oscillates from -0.6 to 0.5 at 0 to 10 sec. After that, it decreased to 0, and then it increased to 0.2 at 50 sec. Then it decreased to – 0.25 at 100 to 150 sec. After that, it increased to 0.2 at 240 sec. Then it decreased to 0 at 250 to 300 sec. The state variables oscillate at 1, 50, 100, 175, and 225. Fig 11 analysis the control input of PID 2 and control input of PID 3 doubly and control Input PID 2 and state variable 2-doubley.

Subplot 11 (a) shows the control input in LFC of PID 2 and PID 3 doubly. The control input PID 1 oscillates -0.7 to 0.5 at 0 to 10 sec. After that, it decreased to 0. Then the oscillation occurs at 50, 100, 175, and 225. At the time of 50, the input oscillates from -0.2 to 0.3, and at the time period of 100, the input oscillates from -0.02 to 0.03. At 175 and 225 sec, the oscillation occurs around -0.1 to 0.1.

Subplot 10 (b) shows the control input in LFC of PID 2 and state variable 2-doubley. Initially, the control input and state variable oscillate from -0.6 to 0.6 at 0 to 10 sec. After that, it decreased to 0, and the state variables and control input oscillated at 50, 100, 175, and 225. The oscillation is very less. Fig 12 Analysis of LFC at the control input of PID 3 and control input of PID 1 doubly and control Input PID 3 and state variable 3-doubley. Subplot 12 (a) shows the control input in LFC of PID 3 and PID 1 doubly.

The control input PID 3 oscillates -0.7 to 0.5 at 0 to 10 sec. After that, it decreased to 0. Then the oscillation occurs at 50, 100, 175, and 225. At the time of 50, the input

oscillates from -0.2 to 0.3, and at the time period of 100, the input oscillates from -0.02 to 0.03. At 175 and 225 sec, the oscillation occurs around -0.1 to 0.1. Subplot 10 (b) shows the control input in LFC of PID 2 and state variable PID -3-doubley. Initially, the control input and state variable oscillate from -0.55 to 0.55 at 0 to 10 sec. After that, it decreased to 0, and the state variables and control input oscillated at 50, 100, 175, and 225. The oscillation is very less.

Analysis of LFC at control input1 and state variable 1, control input 2 and state variable 2, control input3 and state variable 3 are shown in fig 13. Subplot 13 (a) shows the control input1 and state variable 1. The control input is zero at 0 to 300 sec. Initially, it oscillates from 0 to 290 at0 to 10 sec. After that, it increased to 90 at 50 sec. Then it decreased to -125 at 100 to 150 sec. After that, it increased to 90 at 240 sec. Then it decreased to 0 at 250 to 300 sec. Subplot 13 (b) shows the control input 2 and state variable 2. The control input is zero at 0 to 300 sec. The state variable oscillates from -5 to 7 at 0 to 5 sec, then decreases to 0. Then the oscillation occurs at 50, 100, 175, and 225. This oscillation occurs below the -2 to 2 state variable.

Subplot 13 (c) shows the control input 3 and state variable 3. The control input is zero at 0 to 300 sec. Initially, the state variable 3 oscillates from -5 to 7 at 0 to 5 sec, then decreases to 0. Then the oscillation occurs at 50, 100, 175, and 225. This oscillation occurs below the -2 to 2 state variable.

Analysis of LFC using proposed LOA-TFWO Frequency and control input PID 1-doubley is shown in fig 14. The frequency deviation is -0.7 to 0.59 Hz at 0 to 1 sec, after it decreased gradually to 0. Then the frequency deviation occurs at 50, 100, 175, and 225 secs. At 50 sec, the frequency deviation occurs at -0.2 to 0.25 sec. At 100 sec, the oscillation is less than -.01 to 0.1 sec at 175 sec. The oscillation is around -0.1 to 0.1 Hz. At 225 sec, the deviation is around -0.1 to 0.1 Hz.

Using the proposed approach decreases the deviation to a very low value. Fig 15 shows the analysis of frequency deviation and its comparative analysis. Subplot (a) shows the frequency deviation analysis. Frequency deviation is -0.7 to 0.59 Hz at 0 to 1 sec, after it decreased gradually to 0. Then the frequency deviation occurs at 50, 100, 175, and 225 secs. At 50 sec, the frequency deviation occurs at -0.2 to 0.25 sec. At 100 sec, the oscillation is less than -.01 to 0.1 sec at 175 sec. The oscillation is around -0.1 to 0.1 Hz. At 225 sec, the deviation is around -0.1 to 0.1 Hz.

Subplot (b) compares frequency deviation with BMO, SBLA, and COA approaches. This analysis concludes that the proposed approach provides less deviation than the existing approaches.

5.2. Case 2: Performance Analysis of Proposed Approach Based On the System Parameter Change

Analysis of frequency deviation different inertia (H) values is illustrated in fig 16. At increased H values, the frequency deviation is -1.3 to 1.2 Hz at 0 to 1 sec, after it decreased gradually to 0. Then the frequency deviation occurs at 50, 100, 175, and 225 secs. At 50 sec, the frequency deviation occurs at -0.06 to 0.06 sec. At 100 sec, the oscillation is less than -.01 to 0.1 sec at 175 sec. The oscillation is around -0.1 to 0.1 Hz. At 225 sec, the deviation is around -0.1 to 0.1 Hz.

At normal H values, the frequency deviation is -0.6to 0.51 Hz at 0 to 1 sec, after it decreased gradually to 0. Then the frequency deviation occurs at 50, 100, 175, and 225 secs. At 50 sec, the frequency deviation occurs at -0.05 to 0.05 sec. At 100 sec, the oscillation is less than -.01 to 0.01 sec. At 175 sec. The oscillation is around -0.1 to 0.1 Hz. At 225 sec, the deviation is around -0.1 to 0.1 Hz. . At decreased H values, the frequency deviation is -0.7 to 0.7 Hz at 0 to 1 sec, then decreasing gradually to 0. Then the frequency deviation occurs at 50, 100, 175, and 225 secs. At 50 sec, the frequency deviation occurs at -0.05 to 0.05 sec. At 100 sec, the oscillation is less than -.01 to 0.01 sec. At 175 sec. The oscillation is around -0.1 to 0.1 Hz. At 225 sec, the deviation is around -0.1 to 0.1 Hz.

Analysis of frequency deviation with increased inertia (H) values and decrease in H is illustrated in fig 17. Subplot (a) shows the frequency deviation and decrease of H. The frequency deviation is -0.7 to 0.5 Hz at 0 to 1 sec, after it decreased gradually to 0. Then the frequency deviation occurs at 50, 100, 175, and 225 secs. At 50 sec, the frequency deviation occurs at -0.2 to 0.3 sec. At 100 sec, the oscillation is less than -.01 to 0.01 Hz at 175 sec. The oscillation is around -0.1 to 0.1 Hz. At 225 sec, the deviation is around -0.1 to 0.1 Hz. At a decrease of H values, the frequency deviation is -0.39 to 0.3 Hz at 0 to 1sec, after it decreased gradually to 0. Then the frequency deviation occurs at 50, 100, 175, and 225 secs. At 50 sec, the frequency deviation occurs at -0.05 to 0.05 sec. At 100 sec, the oscillation is less than -.01 to 0.01 sec. At 175 sec. The oscillation is around -0.1 to 0.1 Hz. At 225 sec, the deviation is around -0.1 to 0.1 Hz.

Subplot 17 (b) shows H's frequency deviation and increase. The increased H values are -1 to 1.2 at 0 to 1 sec. Then it decreased to 0 at 20 sec. Again, the variation occurs at 50, 100, 175, and 225 secs. At 50 sec, the increase of H values varied from -0.4 to0.5, and at 100 sec, the increase of H values varied from -0.01 to 0.01. At 175 sec, the increase of H values varies from -0.1 to 0.1; at 225 sec, the increase of H values varies from -0.1 to 0.1. The frequency deviation occurs at -0.6 to 0.52 Hz at 0 to 1 sec. Then it decreased to zero, and the deviation was less than the increase in H values.

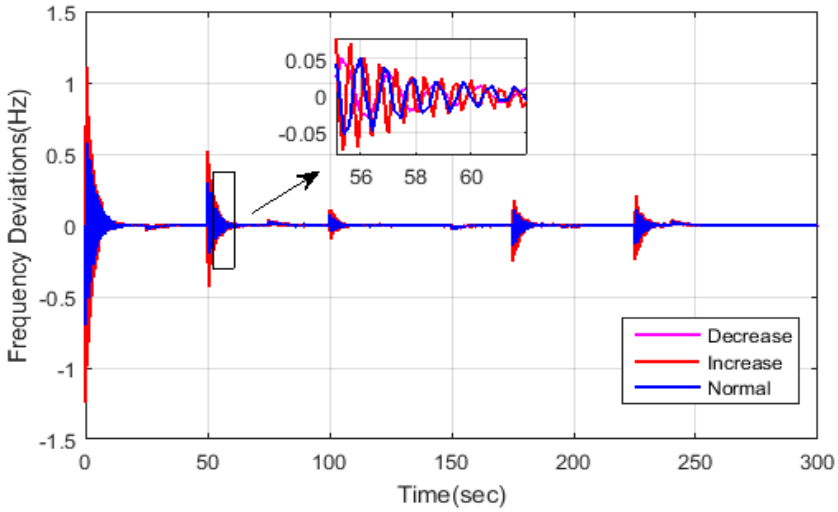

Fig. 16 Analysis of frequency deviation different inertia (H) values

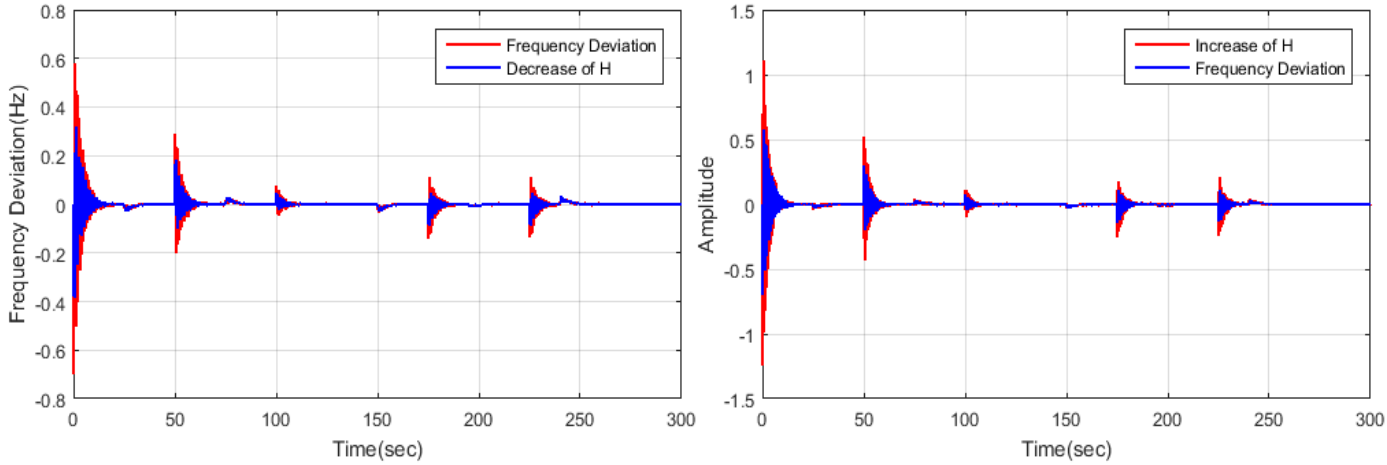

Fig. 17 Analysis of (a) Frequency deviation and decrease of H , (b) Frequency deviation and increase of H

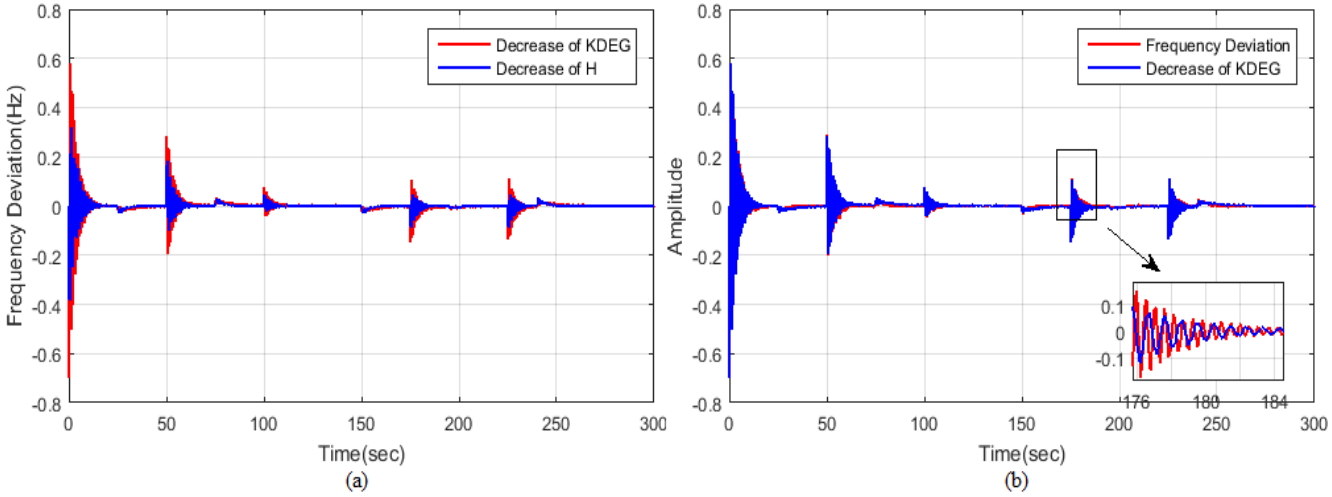

Fig. 18 Analysis of (a) Decrease of H and decrease of K_{DEG}, (b) Decrease of K_{DEG} and frequency deviation

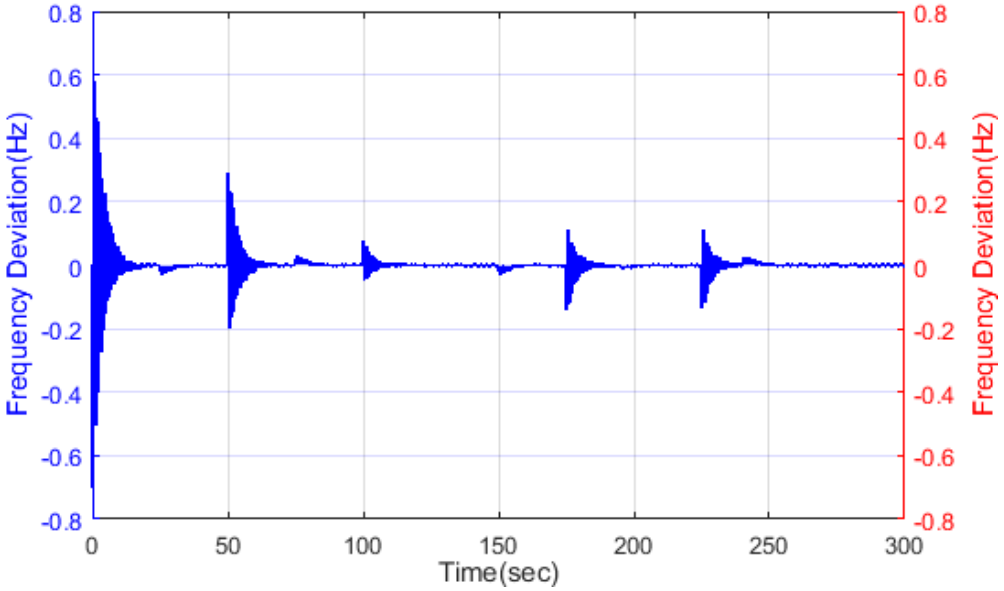

Fig. 19 Analysis of proposed LOA-TFWO frequency and H decrease

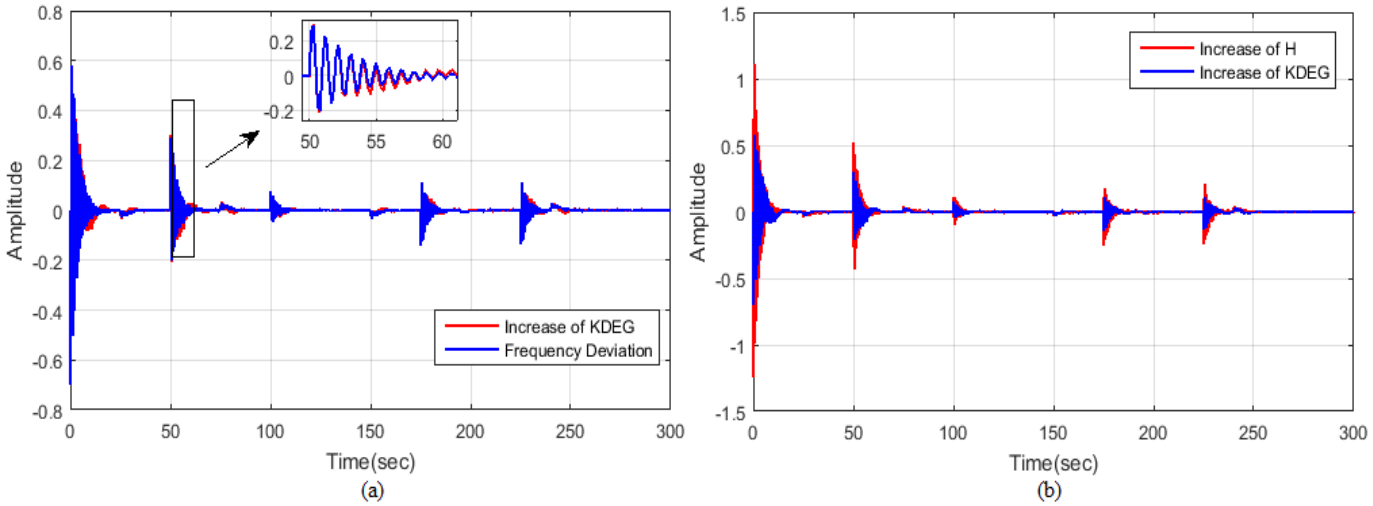

Fig. 20 Analysis of (a) Frequency deviation and increase of K_{DEG} (b) Increase of H and increase of KDEG

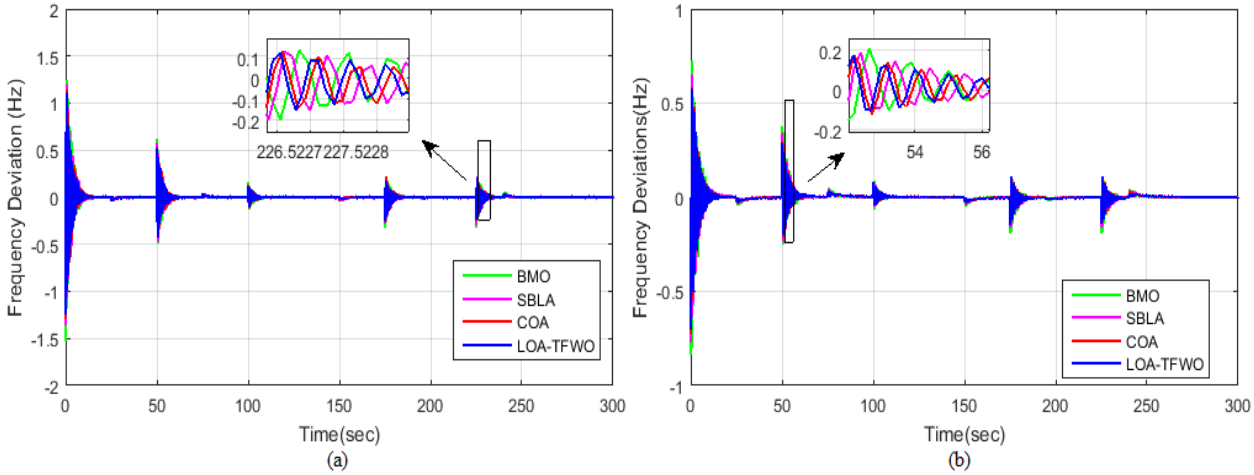

Fig. 21 Analysis of comparison of proposed and existing approaches (a) Frequency deviation increase H values (b) Frequency deviation decrease K_{DEG} values

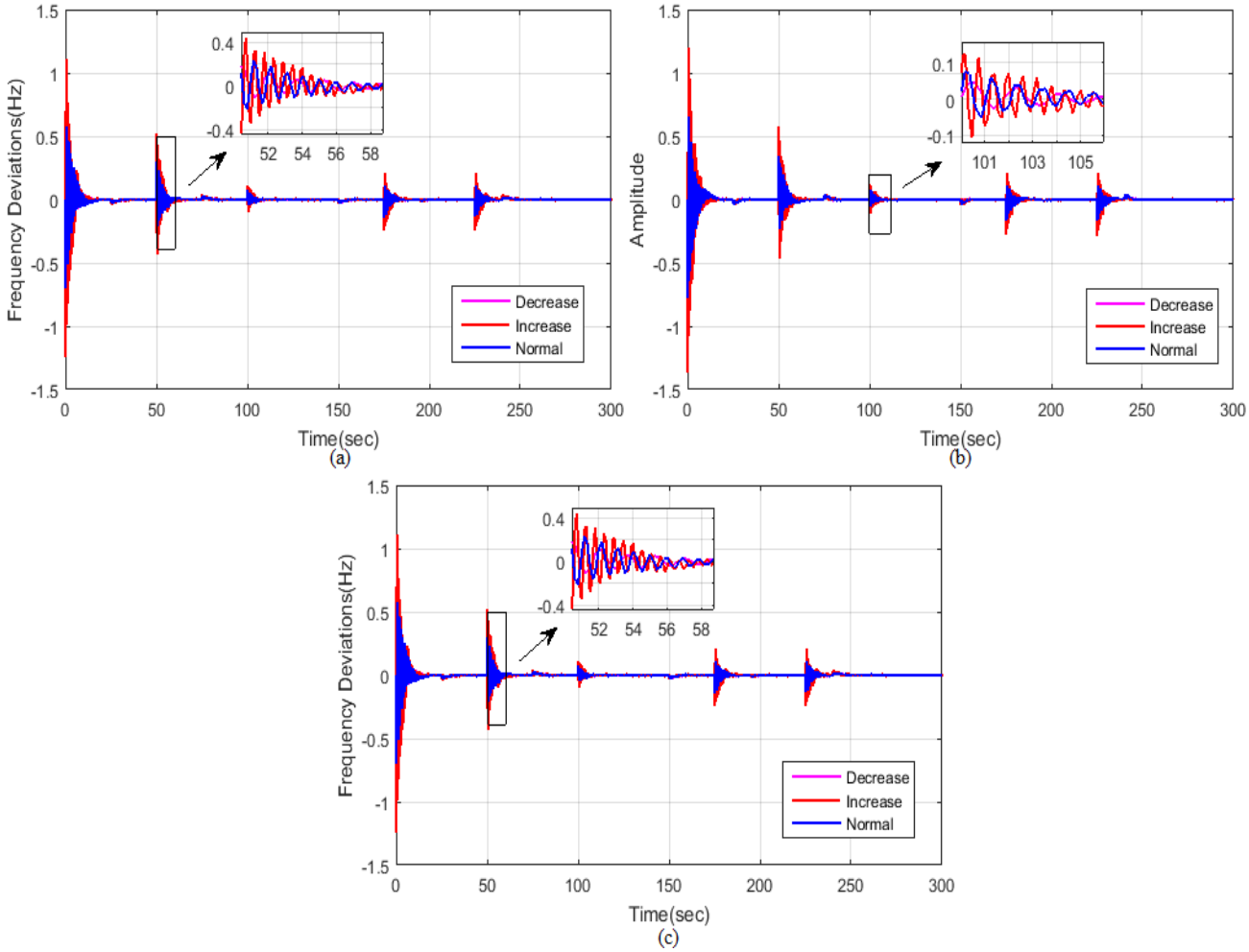

Fig. 22 Analysis of frequency deviation different H values of existing (a) BMO, (b) COA, (c) SBLA

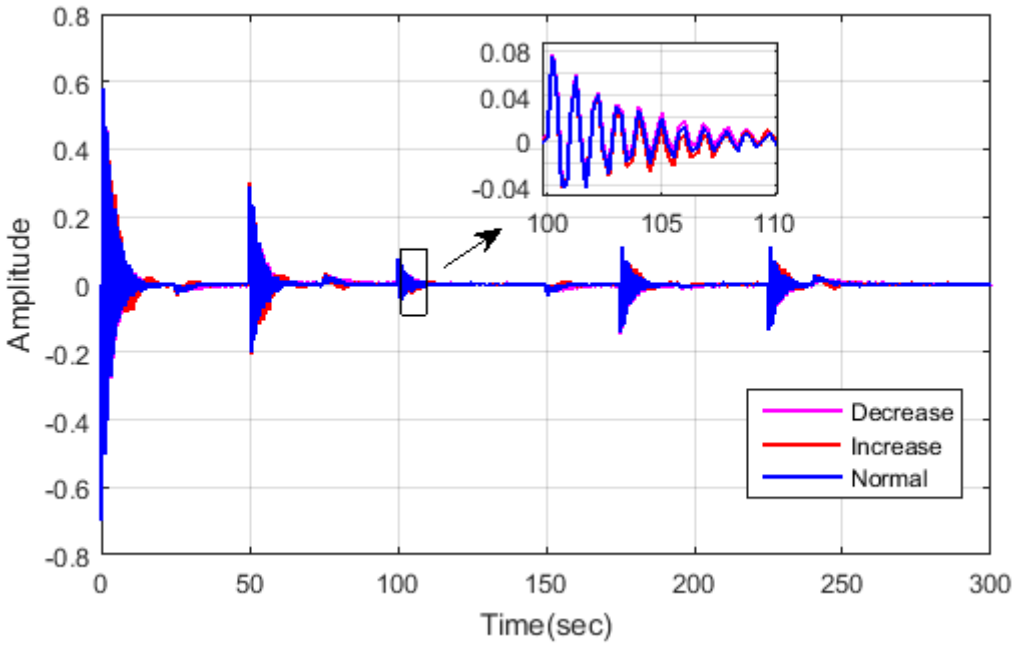

Fig. 23 Analysis of frequency deviation different K_{DEG} Values

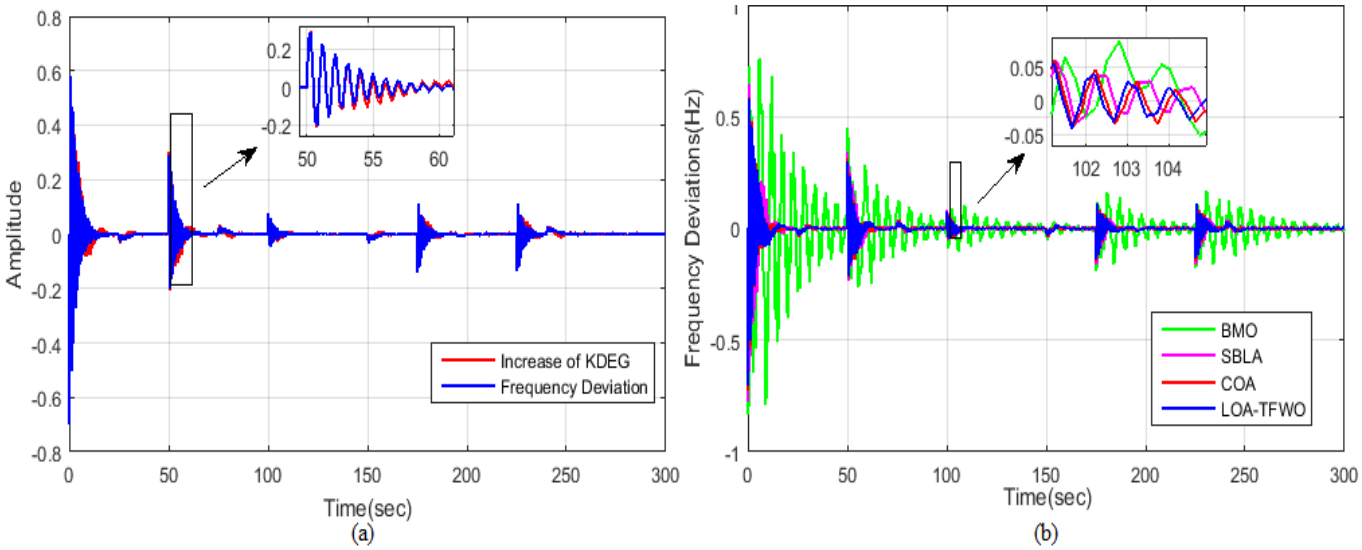

Fig. 24 Analysis of (a) Frequency deviation and increase of K_{DEG}, (b) comparison of frequency deviation increase K_{DEG} values

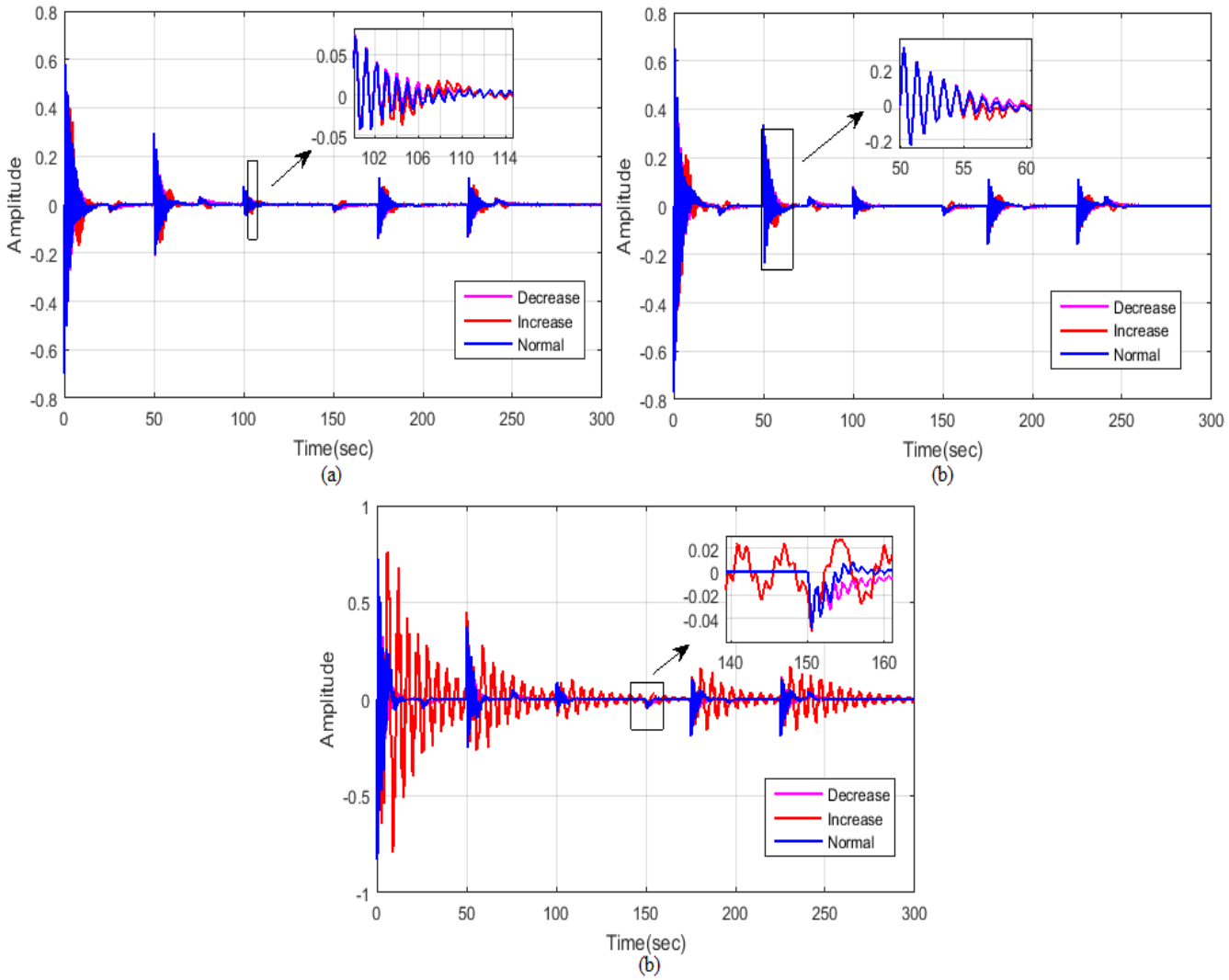

Fig. 25 Analysis of frequency deviation different K_{DEG} values (a) BMO (b) COA (c) SBLA

Analysis of the H and decrease of KDEG and the decrease of K_{DEG} and frequency deviation is shown in fig 18. Subplot 18 (a) shows the analysis of the decrease of H and decrease of K_{DEG}. The decrease of K_{DEG} is varying -0.5 to 0.6 at 0 to 1 sec. Then it decreased to 0 at 20 sec. Again, the variation occurs at 50, 100, 175, and 225 secs. The decrease of K_{DEG} values varies from -0.2 to 0.3 at 50 sec, and at 100 sec, it varies from -0.01 to 0.01. At 175 sec, it varies from -0.1 to 0.1; at 225 sec, the increase of H values varies from -0.1 to 0.1.

H values decrease from -0.4 to 0.32 Hz at 1 sec. Then it decreased to zero, and the deviation was less than the increase in H values. Subplot 18 (b) shows the analysis of frequency deviation and decrease of $K_{DEG.}$ At the analysis of 178 to 184 sec, the frequency deviation is greater than the decrease of K_{DEG} is proved. Analysis of the proposed LOA-TFWO frequency and H decrease is shown in fig 19.

The frequency deviation varies from -0.7 to 0.59 Hz at 0 to 1 sec after decreasing gradually to 0. Then the frequency deviation occurs at 50, 100, 175, and 225 secs. At 50 sec, the frequency deviation occurs at -0.2 to 0.3 sec. At 100 sec, the oscillation is less than -0.01 to 0.01 sec. At 175 sec, the oscillation is around -0.1 to 0.1 Hz. At 225 sec, the deviation is around -0.1 to 0.1 Hz. Analysis of frequency deviation and increase of K_{DEG} and increase of H and increase of K_{DEG} is shown in fig 20.

Subplot (a) shows the analysis of frequency deviation and increase of K_{DEG}. The frequency deviation varies from -0.7 to 0.59 Hz at 0 to 1 sec after decreasing gradually to 0. Then the frequency deviation occurs at 50, 100, 175, and 225 secs. At 50 sec, the frequency deviation occurs at -0.2 to 0.3 sec. At 100 sec, the oscillation is less than -0.01 to 0.01 sec. At 175 sec, the oscillation is around -0.1 to 0.1 Hz. At 225 sec, the deviation is around -0.1 to 0.1 Hz. From this analysis, the frequency deviation and increase of K_{DEG} are similar.

Subplot 20 (b) shows the analysis of the increase of H and the increase of $K_{DEG.}$ The increase in H deviation is higher than the increase in K_{DEG} is proved. Analysis of comparison of proposed and existing approaches at frequency deviation increase H values frequency deviation decrease K_{DEG} values is shown in fig 21. Subplot 21 (a) shows the frequency deviation increase in H values analysis.

At the analysis of the time of 226 to 228 sec, the proposed approach frequency deviation varies from -0.1 to 0.1 Hz, and the existing approaches like BMO, SBLA and COA frequency deviation is a smaller variation than the proposed approaches, it is greater than the -0.1 to 0.1 Hz. So the proposed approach deviates in less value at an increase of H. Subplot 21 (b) shows the analysis of frequency deviation decrease K_{DEG} values.

For analyzing the period of 53 to 56 sec, the proposed approach deviation varies from -0.05 to 0.17 Hz. The existing approaches like BMO, SBLA and COA frequency deviation are higher than the proposed approach. Analysis of frequency deviation of different H Values of existing BMO, COA, and SBLA approaches is shown in fig 22. Subplot 22 (a) shows the BMO approach with various H values.

The frequency deviation analysis at 51 to 58 sec shows that at the normal H values, the deviation is -0.3 to 0.2 Hz. With the increase in H values, the deviation changes from -0.4 to 0.4 Hz, and the decrease in H values changes from -0.3 to 0.35 Hz.

Subplot 22 (b) describes the COA approach frequency deviation; for analyzing at the period of 100 to 105 sec, the increase of H values provides -0.1 to 0.1 Hz frequency deviation

Subplot 22 (c) describes the analysis of the SBLA approach. From this analysis, it is concluded that the higher inertia value means that the deviation is high. Analysis of the frequency deviation of different K_{DEG} Values is shown in fig 23. The frequency deviation analysis at 100 to 110 sec shows that at the normal K_{DEG} values, the deviation is -0.04 to 0.079 Hz. The deviation is almost the same with the increased KDEG values and the decreased KDEG values. Analysis of frequency deviation and increase of K_{DEG}, frequency deviation increase K_{DEG} values are shown in fig 24.

Subplot 22 (b) describes the COA approach frequency deviation; for analyzing at the period of 50 to 60 sec, the increase of K_{DEG} values provides a -0.2 to 0.3 Hz frequency deviation.

Subplot 22 (c) describes the analysis of the SBLA approach. From this analysis, it is concluded that the K_{DEG} value increases means that the deviation is high.

Subplot 24 (a) shows the frequency deviation and increase of K_{DEG}. The deviation and the increase of K_{DEG} is a small point variation at 50 to 60 sec. Subplot 24 (b) compares frequency deviation increase K_{DEG} values. From that comparison, the proposed approach deviation is less than the existing approaches like BMO, COA, and SBLA. Analysis of frequency deviation of different K_{DEG} values BMO, COA, and SBLA is shown in fig 25.

Subplot 25 (a) shows the BMO approach with various K_{DEG} values. The frequency deviation analysis at 102 to 115 sec shows that at the normal K_{DEG} values, the deviation is -0.05 to 0.05 Hz, and at the increased K_{DEG} values, the deviation changes from -0.05 to 0.04 Hz; the decreased K_{DEG} values, the deviation is changing from -0.04 to 0.35 Hz.

Table 1. Comparison of proposed and existing approaches using simulation [44]

Parameter	Maximum overshoot (Hz)	Steady-state error (Hz)	Maximum settling time (sec)	Integral frequency errors the absolute value in the simulation period $\int_0^T \Delta f(T)dT$	Objective function
Without Control	0.5033	4739×10^{-6}	50	60.8298	309567.5
PID	0.0188	47.4×10^{-6}	17	0.2751	29841.6
ABC approach	0.0127	3.04×10^{-6}	2.5	0.0489	26794.3
Proposed approach	0.0121	2.98×10^{-6}	2.1	0.0476	25793.2

A comparison of proposed and existing approaches using simulation is tabulated in table 1. The table analyzed the maximum overshoot, steady state error, maximum settling time, integral of frequency error's absolute value in the simulation period, and objective function.

From this analysis, the proposed approach's maximum overshoot is 0.0121 Hz, less than the ABC, PID without the controller. The settling time of the proposed approach is 2.1 sec. From this analysis, the proposed approach provides a better outcome than the existing approach.

6. Conclusion

This paper proposed a hybrid LOA-TFWO approach for the LFC of the standalone microgrid. The LOA approach generates the data set, and the TFWO approach is utilized to optimize the objective function. The standalone microgrid system combines many sources like PV, WT, FC, BESS, and DEG. Three PID controllers are utilized for tuning the parameter of the proposed system.

The proposed approach performance is analyzed based on the state and control variable variation and the parameter change. The proposed approach decreases the change of frequency against large load/generation fluctuations. The proposed approach characteristics are verified using maximum overshoot, maximum steady-state error, maximum settling time, and integral of frequency error's absolute value. The proposed approach is compared to existing approaches like BMO, COA, and SBLA. From that comparison, it is depicted that the proposed approach's performance is superior to the existing approaches.

References

[1] Z. Yan and Y. Xu, "A Multi-Agent Deep Reinforcement Learning Method for Cooperative Load Frequency Control of a Multi-Area Power System," *IEEE Transactions on Power Systems*, vol.35, no.6, pp.4599-4608, 2020.

[2] M. Ma, C. Zhang, X. Liu and H. Chen, "Distributed Model Predictive Load Frequency Control of the Multi-Area Power System After Deregulation," *IEEE Transactions on Industrial Electronics*, vol.64, no.6, pp.5129-5139, 2017.

[3] L. Cai, Z. He and H. Hu, "A New Load Frequency Control Method of Multi-Area Power System Via the Viewpoints of Port-Hamiltonian System and Cascade System," *IEEE Transactions on Power Systems*, vol.32, no.3, pp.1689-1700, 2017.

[4] E. Sahin, "Design of an Optimized Fractional High Order Differential Feedback Controller for Load Frequency Control of a Multi-Area Multi-Source Power System with Non-Linearity," *IEEE Access*, vol.8, pp.12327-12342, 2020.

[5] H. Li, X. Wang and J. Xiao, "Adaptive Event-Triggered Load Frequency Control for Interconnected Microgrids By Observer-Based Sliding Mode Control," *IEEE Access*, vol.7, pp.68271-68280, 2019.

[6] X. Lv, Y. Sun, Y. Wang and V. Dinavahi, "Adaptive Event-Triggered Load Frequency Control of Multi-Area Power Systems Under Networked Environment Via Sliding Mode Control," *IEEE Access*, vol.8, pp.86585-86594, 2020.

[7] S. Hanwate, Y. Hote and S. Saxena, "Adaptive Policy for Load Frequency Control," *IEEE Transactions on Power Systems*, vol.33, no.1, pp.1142-1144, 2018.

[8] V. Singh, N. Kishor and P. Samuel, "Distributed Multi-Agent System-Based Load Frequency Control for Multi-Area Power System In Smart Grid," *IEEE Transactions on Industrial Electronics*, vol.64, no.6, pp.5151-5160, 2017.

[9] X. Zhou, Z. Gu and F. Yang, "Resilient Event-Triggered Output Feedback Control for Load Frequency Control Systems Subject To Cyber Attacks," *IEEE Access*, vol.7, pp.58951-58958, 2019.

[10] P. Babahajiani, Q. Shafiee and H. Bevrani, "Intelligent Demand Response Contribution in Frequency Control of Multi-Area Power Systems," *IEEE Transactions on Smart Grid*, vol.9, no.2, pp.1282-1291, 2018.

[11] G. Chen, Z. Li, Z. Zhang and S. Li, "An Improved Aco Algorithm Optimized Fuzzy Pid Controller for Load Frequency Control In Multi Area Interconnected Power Systems," *IEEE Access*, vol.8, pp.6429-6447, 2020.

[12] C. Peng, J. Li and M. Fei, "Resilient Event-Triggering $H_{\Infty }$ Load Frequency Control for Multi-Area Power Systems with Energy-Limited Dos Attacks," *IEEE Transactions on Power Systems*, vol.32, no.5, pp.4110-4118, 2017.

[13] Y. Zhang and T. Yang, "Decentralized Switching Control Strategy for Load Frequency Control In Multi-Area Power Systems with Time Delay and Packet Losses," *IEEE Access*, vol.8, pp.15838-15850, 2020.
[14] P. Ojaghi and M. Rahmani, "Lmi-Based Robust Predictive Load Frequency Control for Power Systems with Communication Delays," *IEEE Transactions on Power Systems*, vol.32, no.5, pp.4091-4100, 2017.
[15] Z. Li, X. Li and B. Cui, "Planar Clouds Based Load Frequency Control in Interconnected Power System with Renewable Energy," *IEEE Access*, vol.6, pp.36459-36468, 2018.
[16] L. Jin, C. Zhang, Y. He, L. Jiang and M. Wu, "Delay-Dependent Stability Analysis of Multi-Area Load Frequency Control with Enhanced Accuracy and Computation Efficiency," *IEEE Transactions on Power Systems*, vol.34, no.5, pp.3687-3696, 2019.
[17] F. Yang, J. He and Q. Pan, "Further Improvement on Delay-Dependent Load Frequency Control of Power Systems Via Truncated B–L Inequality," *IEEE Transactions on Power Systems*, vol.33, no.5, pp.5062-5071, 2018.
[18] Y. Zhang, X. Liu and B. Qu, "Distributed Model Predictive Load Frequency Control of Multi-Area Power System with Dfigs," *IEEE/Caa Journal of Automaticasinica*, vol.4, no.1, pp.125-135, 2017.
[19] Y. Wu, Z. Wei, J. Weng, X. Li and R. Deng, "Resonance Attacks on Load Frequency Control of Smart Grids," *IEEE Transactions on Smart Grid*, vol.9, no.5, pp.4490-4502, 2018.
[20] Y. Bao, Y. Li, B. Wang, M. Hu and P. Chen, "Demand Response for Frequency Control of Multi-Area Power System," *Journal of Modern Power Systems and Clean Energy*, vol.5, no.1, pp.20-29, 2017.
[21] K. Lu, W. Zhou, G. Zeng and Y. Zheng, "Constrained Population Extremal Optimization-Based Robust Load Frequency Control of Multi-Area Interconnected Power System," *International Journal of Electrical Power & Energy Systems*, vol.105, pp.249-271, 2019
[22] H. Hasanien and A. El-Fergany, "Salp Swarm Algorithm-Based Optimal Load Frequency Control of Hybrid Renewable Power Systems with Communication Delay and Excitation Cross-Coupling Effect," *Electric Power Systems Research*, vol.176, pp.105938, 2019.
[23] H. Hasanien and A. El-Fergany, "Salp Swarm Algorithm-Based Optimal Load Frequency Control of Hybrid Renewable Power Systems with Communication Delay and Excitation Cross-Coupling Effect," *Electric Power Systems Research*, vol.176, pp.105938, 2019.
[24] B. Sonker, D. Kumar and P. Samuel, "Dual Loop Imc Structure for Load Frequency Control Issue of Multi-Area Multi-Sources Power Systems," *International Journal of Electrical Power & Energy Systems*, vol.112, pp.476-494, 2019.
[25] P. Sahu, S. Mishra, R. Prusty and S. Panda, "Improved-Salp Swarm Optimized Type-Ii Fuzzy Controller In Load Frequency Control of Multi Area Islanded Ac Microgrid," *Sustainable Energy, Grids and Networks*, vol.16, pp.380-392, 2018.
[26] A. Abazari, H. Monsef and B. Wu, "Coordination Strategies of Distributed Energy Resources Including Fess, Deg, Fc and Wtg In Load Frequency Control (Lfc) Scheme of Hybrid Isolated Micro-Grid," *International Journal of Electrical Power & Energy Systems*, vol.109, pp.535-547, 2019.
[27] Y. Sun, Y. Wang, Z. Wei, G. Sun and X. Wu, "Robust H∞ Load Frequency Control of Multi-Area Power System with Time Delay: A Sliding Mode Control Approach," *IEEE/Caa Journal of Automaticasinica*, vol.5, no.2, pp.610-617, 2018
[28] M. Khooban, T. Niknam, F. Blaabjerg and T. Dragičević, "A New Load Frequency Control Strategy for Micro-Grids with Considering Electrical Vehicles," *Electric Power Systems Research*, vol.143, pp.585-598, 2017.
[29] K. Rajesh and S. Dash, "Load Frequency Control of Autonomous Power System Using Adaptive Fuzzy Based Pid Controller Optimized on Improved Sine Cosine Algorithm," *Journal of Ambient Intelligence and Humanized Computing*, vol.10, no.6, pp.2361-2373, 2018.
[30] M. Chen, G. Zeng and X. Xie, "Population Extremal Optimization-Based Extended Distributed Model Predictive Load Frequency Control of Multi-Area Interconnected Power Systems," *Journal of the Franklin Institute*, vol.355, no.17, pp.8266-8295, 2018.
[31] A. Dabiri, B. Moghaddam and J. Machado, "Optimal Variable-Order Fractional Pid Controllers for Dynamical Systems," *Journal of Computational and Applied Mathematics*, vol.339, pp.40-48, 2018
[32] D. Li, L. Liu, Q. Jin and K. Hirasawa, "Maximum Sensitivity Based Fractional Imc–Pid Controller Design for Non-Integer Order System with Time Delay," *Journal of Process Control*, vol.31, pp.17-29, 2015.
[33] L. Liu, F. Pan and D. Xue, "Variable-Order Fuzzy Fractional Pid Controller," *Isa Transactions*, vol.55, pp.227-233, 2015.
[34] G. Zeng, J. Chen, Y. Dai, L. Li, C. Zheng and M. Chen, "Design of Fractional Order Pid Controller for Automatic Regulator Voltage System Based on Multi-Objective Extremal Optimization," *Neurocomputing*, vol.160, pp.173-184, 2015.
[35] M. Khosraviani, M. Jahanshahi, M. Farahani and A. Bidaki, "Load–Frequency Control Using Multi-Objective Genetic Algorithm and Hybrid Sliding Mode Control-Based Smes," *International Journal of Fuzzy Systems*, vol.20, no.1, pp.280-294, 2017.
[36] G. Nguyen, K. Jagatheesan, A. Ashour, B. Anand and N. Dey, "Ant Colony Optimization Based Load Frequency Control of Multi-Area Interconnected Thermal Power System with Governor Dead-Band Nonlinearity," *Lecture Notes In Networks and Systems*, pp.157-167, 2017.
[37] C. Peng, J. Zhang and H. Yan, "Adaptive Event-Triggering ${H}_{\Infty }$ Load Frequency Control for Network-Based Power Systems," *IEEE Transactions on Industrial Electronics*, vol.65, no.2, pp.1685-1694, 2018

[38] J. Mudi, C. Shiva and V. Mukherjee, "Multi-Verse Optimization Algorithm for Lfc of Power System with Imposed Non-Linearities Using Three-Degree-of-Freedom Pid Controller*," Iranian Journal of Science and Technology, Transactions of Electrical Engineering*, vol.43, no.4, pp.837-856, 2019.

[39] C. Mu, Y. Tang and H. He, "Improved Sliding Mode Design for Load Frequency Control of Power System Integrated an Adaptive Learning Strategy," *IEEE Transactions on Industrial Electronics*, vol.64, no.8, pp.6742-6751, 2017.

[40] P. Ojaghi and M. Rahmani, "Lmi-Based Robust Predictive Load Frequency Control for Power Systems with Communication Delays," *IEEE Transactions on Power Systems*, vol.32, no.5, pp.4091-4100, 2017.

[41] M. Mohamed, A. Diab, H. Rezk and T. Jin, "A Novel Adaptive Model Predictive Controller for Load Frequency Control of Power Systems Integrated with Dfig Wind Turbines," *Neural Computing and Applications*, vol.32, no.11, pp.7171-7181, 2019.

[42] G. Shankar and V. Mukherjee, "Quasi Oppositional Harmony Search Algorithm Based Controller Tuning for Load Frequency Control of Multi-Source Multi-Area Power System," *International Journal of Electrical Power & Energy Systems*, vol.75, pp.289-302, 2016.

[43] J. Pereira, M. Francisco, S. Cunha Jr. and G. Gomes, "A Powerful Lichtenberg Optimization Algorithm: A Damage Identification Case Study," *Engineering Applications of Artificial Intelligence*, vol.97, pp.104055, 2021.

[44] M. Ghasemi, I. Davoudkhani, E. Akbari, A. Rahimnejad, S. Ghavidel and L. Li, "A Novel and Effective Optimization Algorithm for Global Optimization and Its Engineering Applications: Turbulent Flow of Water-Based Optimization (Tfwo)," *Engineering Applications of Artificial Intelligence*, vol.92, pp.103666, 2020.

[45] A. Bagheri, A. Jabbari and S. Mobayen, "An Intelligent Abc-Based Terminal Sliding Mode Controller for Load-Frequency Control of Islanded Micro-Grids," *Sustainable Cities and Society*, vol.64, pp.102544, 2021.

[46] Dr. S. Deepa, Lavanya Dhanesh, P.Elangovan, "Optimal Fuzzy Controller for Power Quality Improvement of Dynamic Voltage Restorer Using Bacterial Foraging Algorithm," *International Journal of Advanced Science and Technology*, vol.28, no.19, pp.10-15 , 2019.

[47] Dr.S.Deepa ,"A Fuzzy Ga Based Statcom for Power Quality Improvement," *International Journal of Power Electronics and Drives*, vol.8, no.1, pp.483-491, 2017.